AD-A097 440 HARRY DIAMOND LABS ADELPHI MD F/G 19/1
A TECHNIQUE TO MEASURE OSCILLATOR SENSITIVITY.(U)
FEB 81 N D WILKIN
UNCLASSIFIED HDL-TM-81-3 NL

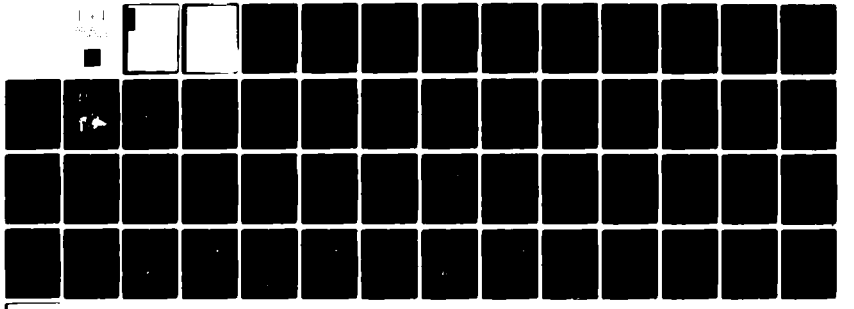

END
DATE FILMED
5-81
DTIC

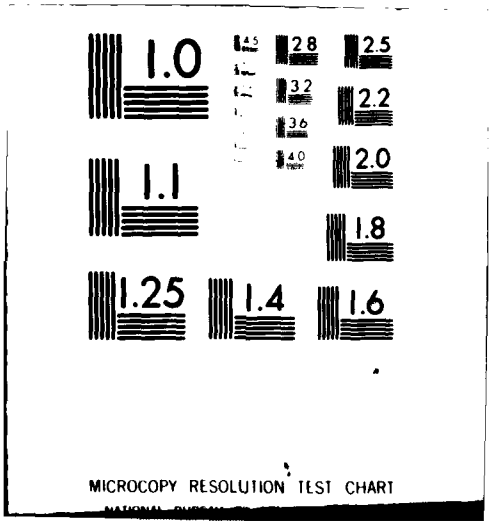
1.0
1.1
1.25
1.4
1.6
1.8
2.0
2.2
2.5
2.8
3.2
3.6
4.0
MICROCOPY RESOLUTION TEST CHART

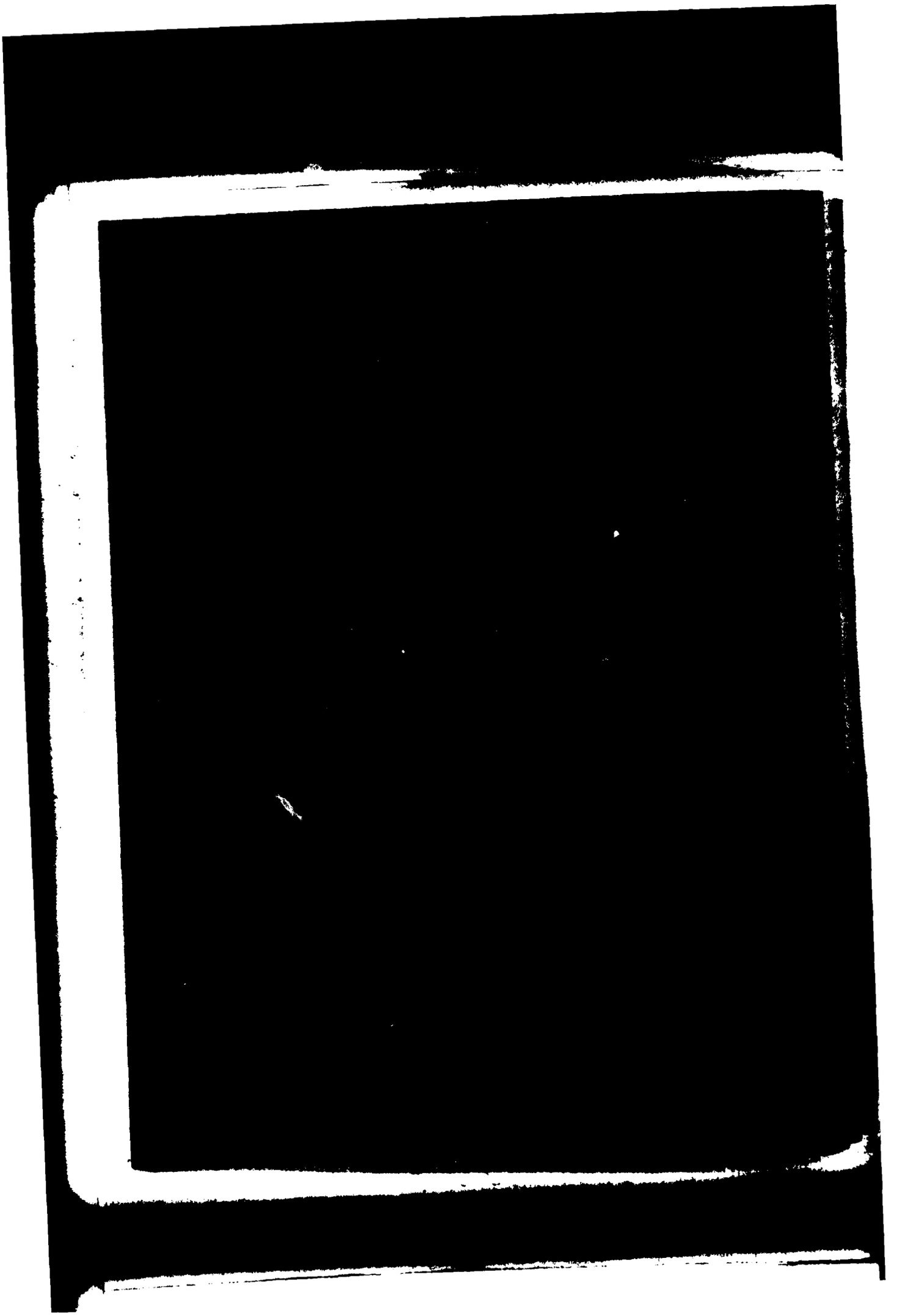

UNCLASSIFIED

SECURITY CLASSIFICATION OF THIS PAGE (When Data Entered)

REPORT DOCUMENTATION PAGE	READ INSTRUCTIONS BEFORE COMPLETING FORM
REPORT NUMBER: HDL-TM-81-3	2. GOVT ACCESSION NO.: AD-A097440
3. RECIPIENT'S CATALOG NUMBER	
4. TITLE (and Subtitle): A Technique to Measure Oscillator Sensitivity.	5. TYPE OF REPORT & PERIOD COVERED: Technical Memorandum
	6. PERFORMING ORG. REPORT NUMBER
7. AUTHOR(s): Neil D. Wilkin	8. CONTRACT OR GRANT NUMBER(s): PEMA No. 4932 MMT No. 5733048/5743048
9. PERFORMING ORGANIZATION NAME AND ADDRESS: Harry Diamond Laboratories 2800 Powder Mill Road Adelphi, MD 20783	10. PROGRAM ELEMENT, PROJECT, TASK AREA & WORK UNIT NUMBERS
11. CONTROLLING OFFICE NAME AND ADDRESS: US Army Materiel Development and Readiness Command Alexandria, VA 22333	12. REPORT DATE: Feb 1981 13. NUMBER OF PAGES: 54
14. MONITORING AGENCY NAME & ADDRESS (if different from Controlling Office)	15. SECURITY CLASS. (of this report): UNCLASSIFIED 15a. DECLASSIFICATION/DOWNGRADING SCHEDULE

16. DISTRIBUTION STATEMENT (of this Report)

Approved for public release; distribution unlimited.

17. DISTRIBUTION STATEMENT (of the abstract entered in Block 20, if different from Report)

18. SUPPLEMENTARY NOTES

HDL Project No. 141312 and 141412

19. KEY WORDS (Continue on reverse side if necessary and identify by block number)

Fuze	Anechoic chamber
Sensitivity	Test chamber
Oscillator detector	Loop antenna standard
Radiated power	Pole test replacement
Fuze sensitivity	Detector sensitivity

20. ABSTRACT (Continue on reverse side if necessary and identify by block number)

A study of oscillator sensitivity measurement employing a small anechoic chamber is described. Sensitivity is measured in a small (0.91 m^3) chamber suitable for production-line fuze testing. Since the measurement is absolute, no reference is necessary to a pole test facility, as previous test chambers required. The sensitivity measurement technique replaces the pole test as the standard measurement technique and can be

DD FORM 1 JAN 73 1473 EDITION OF 1 NOV 65 IS OBSOLETE

UNCLASSIFIED

SECURITY CLASSIFICATION OF THIS PAGE (When Data Entered)

163050

20. ABSTRACT (Cont'd)

performed in small or large anechoic chambers. An error analysis is included, and the estimated measurement error in the small chamber is 10.4 percent. A shortened procedure is described which permits 100-percent production-line testing for fuze sensitivity and radiated power. Admittance data, radiation patterns, and gain data for standard loop antennas used in calibration are also presented.

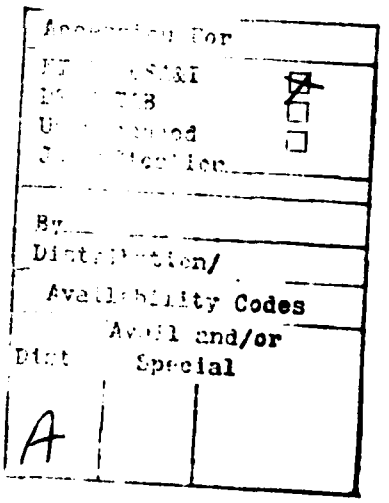

CONTENTS

FIGURES

FIGURES (Cont'd)

1. INTRODUCTION

The standard measurement procedure for determining oscillator sensitivity of radio proximity fuzes has historically been the pole test. The fuze under test was moved either towards or away from a large reflecting screen while the detector voltage was monitored. Generally, the apparatus for moving the fuze consisted of a pole and a hoist; thus, the procedure became known as a "pole test." Little was known about its accuracy, except that intuitively it seems to simulate the "actual use" situation. Errors such as those due to finite screen size and the effects of reflections from the pole and hoist apparatus were ignored or considered minimal. A long-standing clue that these errors may be significant has been the difference in test results when the same fuzes were measured on different pole test facilities. Measurements varying as much as 2 to 1 have been obtained in extreme cases. Two other problems with the outdoor pole testing are the lack of security for the system under test, and the limitation on the test to days of fair weather.

As a companion to the pole test, for laboratory or production-line testing, small loading and unloading chambers have been used. These chambers employed either mechanically rotating or electronically switched dipoles to induce a reflecting signal into the oscillator. The chambers are calibrated over a frequency range by direct comparison with the pole test.

This paper describes an improved technique for sensitivity measurement employing a small anechoic chamber in which the errors can be computed or measured. It is the same technique as described by Wilkin (1972).[1] That report describes measurements made in a large anechoic chamber. In this report the accuracy of the method when applied to a relatively small chamber is discussed.

The fuze under test is fixed in a small anechoic chamber. Sensitivity is determined by first measuring the fuze radiated power, and then, after accounting for all losses in the system, "playing back" a signal to the fuze in a magnitude which simulates a given height above an infinite plane reflector at a prescribed reflection coefficient. The fuze detector's response to this signal is recorded as a measure of fuze sensitivity.

Four areas were studied during this project: refinements to the basic test technique, standard loop antenna fabrication and calibration, characteristics of the small anechoic chamber, and system errors. Each area is covered in a separate section of this report.

---

[1] *Neil D. Wilkin, An Absolute Measurement Procedure to Determine Oscillator-Detector Sensitivity and Power, Harry Diamond Laboratories, HDL-TR-1606 (April 1972).*

2. DESCRIPTON OF TECHNIQUE

2.1 Basic Method

The absolute measurement procedure is outlined so that the reader may understand the technique. A shortened procedure will become apparent and is described later.

The fuze oscillator detector under test is placed at one end of an anechoic chamber, preferably at the end with the largest quiet zone. At the opposite end, an antenna A_3 is placed so that a portion of the oscillator signal can be received and measured, so that a processed signal can be returned to the oscillator (fig. 1). An additional antenna is used to sample the oscillator signal--this sample to be used as the input signal to the signal processor. The signal processor is a frequency-offset generator (single-sideband technique) which varies the phase and then amplifies the signal for return via A_3 to the oscillator. In an alternative procedure, the signal processor is replaced with a standard signal generator, and the oscillator is allowed to "lock in" to the generator frequency. The lock-in response of the oscillator is recorded as the generator frequency is varied. This latter method can be applied only to unmodulated oscillator systems. The magnitude of the processed signal is set so that the oscillator is presented with a field equal to a value corresponding to a desired height above an infinite perfect reflector. This desired field strength is the result of the forward power P_f from the processor, as in figure 1, and the relationship between this power and the field can be determined as follows.

One may start by defining the space loss L_s as the ratio of the available return signal power* P at the oscillator to the power P_{A3}, which is the net power delivered to the terminals of antenna A_3 (fig. 1). For reciprocal transmission, this space loss holds for the test setup shown in figure 2. Thus, we can also write the space loss as the ratio of the available power P_{D3} to the power P_1 radiated by the antenna A_1 of the oscillator. Hence,

$$L_s = \frac{P}{P_{A3}} = \frac{P_{D3}}{P_1} \quad . \tag{1}$$

The available power, P, is equal to the return signal power density at the fuze multiplied by the receiving cross section of the oscillator antenna.

When the oscillator is turned on, the power P_3 is measured (fig. 2). Then the oscillator is removed from the chamber and replaced with a standard antenna A_2 in the same physical location. The absolute gain of antenna A_2 must be known. The oscillator frequency and the power P_3 can then be duplicated by adjustment of the signal generator shown in figure 3. Thus we may equate the power-gain products

$$P_1 G_1 = P_2 G_2 \quad . \tag{2}$$

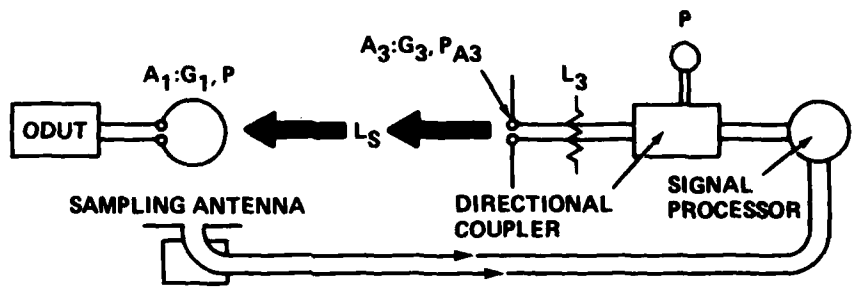

Figure 1. Return-signal test setup.

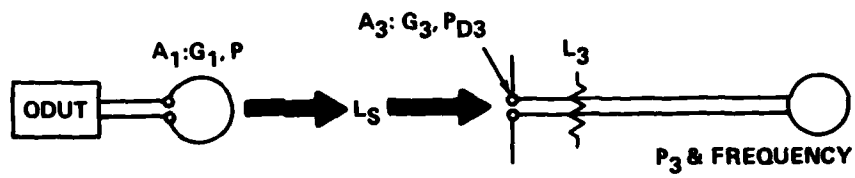

Figure 2. Oscillator radiated-power test setup.

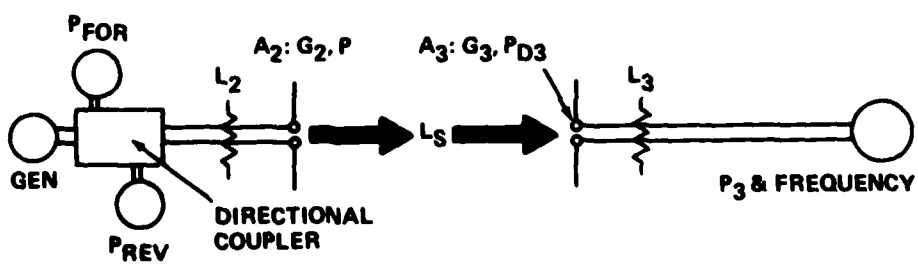

Figure 3. Oscillator radiated-power simulation test setup.

G_1 and G_2 are the power gains for antennas A_1 and A_2, respectively. P_2 is the net power radiated by antenna A_2 or

$$P_2 = L_2 P_{for} - P_{rev}/L_2 \quad . \tag{3}$$

P_{for} and P_{rev} are the forward and reverse power, respectively, in the transmission line, as measured through the directional coupler. L_2 is the match line loss of the coaxial cable. P_{D3} can be related to P_3 by the following equation,

$$P_3 = P_{D3} L_3 (1 - \Gamma^2) \quad , \tag{4}$$

which includes the antenna mismatch parameter, Γ^2, and the transmission line loss, L_3. The power meter used here is assumed to be well matched to the line. L_s can now be calculated by combining equations (1) through (4):

$$L_s = \frac{P_{D3}}{P_1} = \frac{G_1 P_3}{L_3 G_2 P_2 (1 - \Gamma^2)} \quad . \tag{5}$$

To simulate a particular height above ground, $P_{A3} L_s$ is set equal to $P_1 L_h$, where L_h is the two-way transmission loss between antenna A_1 and an infinite reflector with a reflection coefficient of unity. Thus,

$$L_h = \left(\frac{G_1 C}{8\pi h f}\right)^2 \quad . \tag{6}$$

C is the speed of light in free space, h is the height to be simulated, and f is the operating frequency. P_{A3} is related to P_f (fig. 1) by

$$P_{A3} = P_f L_3 (1 - \Gamma^2) \quad , \tag{7}$$

where P_f is the forward return signal power at the directional coupler.

Forming $P_{A3}L_s = P_1L_h$, from the equations above, and then solving for P_f, we arrive at the desired result:

$$P_f = \frac{P_2^2}{P_3}\left(\frac{G_2C}{8\pi hf}\right)^2 \quad . \tag{8}$$

Thus, equation (8) gives the power P_f necessary to make the magnitude of the return signal identical to that for an oscillator suspended at a height h above an infinite reflector.

One needs only to vary the return signal phase to determine the detector response after the magnitude of P_f has been set. If the phase is varied through 360 degrees, the resultant peak-to-peak detector voltage swing is equal to the magnitude of the Doppler envelope at height h. One should note that the oscillator antenna gain G_1, the mismatch losses $(1 - \Gamma^2)$ of antenna A_3, and the loss L_3 in the cable connecting A_3 to the power meter do not enter the equation. Of prime importance, however, is the standard antenna gain G_2. The accuracy of the measurements depends on how well this is known.

On occasion, the laboratory equipment may not provide sufficient return signal power to simulate a given height above the reflector. Since the detector voltage is directly proportional to the square root of the return signal power, one can set the return signal magnitude to any convenient value and calculate the detector response E_h for the desired height h. The resulting equation is as follows:

$$E_h = E_m\left(\frac{G_2C}{8\pi hf}\right)\frac{P_2}{\left(P_f'P_3\right)^{1/2}} \quad , \tag{9}$$

where E_m is the measured detector response due to the actual forward return signal power, P_f'.

2.2 Technique Refinement

For production-line testing, a shortened procedure becomes available if the chamber is once calibrated over the frequency range of interest. Equation (9) may be rewritten as

$$E_h = E_m\left(\frac{P_3}{P_f}\right)^{1/2}\left(\frac{P_2}{P_3}\right)\left(\frac{G_2C}{8\pi hf}\right) \quad . \tag{10}$$

Define the ratio P_3/P_2 as the transmission loss L(f) of the chamber. L(f) can be measured over the frequency range of interest using the standard antenna in the test setup of figure 3. E_h can then be calculated from

$$E_h = E_m \left(\frac{P_3}{P_f'}\right)^{1/2} \left[\frac{1}{L(f)}\right] \left(\frac{G_2 C}{8\pi hf}\right) \quad , \tag{11}$$

$1/L(f)$ and $G_2C/8\pi hf$ can be combined and tabulated versus frequency. Correction factors for measurements of E_m, P_3, and P_f' due to high impedance cable, transmission-line, and switching-circuit losses that are not considered in the procedure can also be included in the tabulation.

The radiated P_{rad} of the oscillator can also be calculated by combining equations (2) and (11). Hence,

$$P_{rad} = P_1 \frac{G_2 P_3}{G_1 L(f)} \quad . \tag{12}$$

Thus, the basic method can be shortened by precalibrating the anechoic chamber and plotting all factors for losses and other corrections together versus frequency. This shortened method can be applied to any chamber and is still an absolute measurement: the calibration technique is based on standard measurements and does not need to be checked against any other type of sensitivity measurement system.

3. STANDARD ANTENNA (A_2) CONSIDERATIONS

To insure accuracy of measurements using this technique, care must be exercised in the selection of the standard antenna, A_2, particularly when the measurements are performed in a small anechoic chamber. Greater accuracy is obtained when a standard antenna is of the same type as that of the fuze (for example, a loop standard for a loop fuze). Use of a dipole standard when measuring a loop-antenna fuze may introduce errors in the estimate of chamber attenuation, because different reflecting paths come into play when the antennas are of the same polarization and radiation pattern. The problem is generally more acute when a small anechoic chamber is used, because of the greater importance of reflecting paths. On the other hand, if the measurements were made in free space, the type of standard antenna would be unimportant so long as the absolute gain were known.

Standard dipole antennas are readily available, but standard loop antennas with 50-ohm drive impedance and known gain charaterizations are unavailable commercially. As a result, Harry Diamond Laboratories (HDL) has designed and fabricated a unique loop antenna for use as a standard. Each antenna has a bandwidth of approximately 35 MHz. Two sets of four antennas were fabricated, the second set serving as a spare.

Each loop antenna is designed to have a 50-ohm radiation resistance by determining its diameter according to[2]

$$D = \left(R_r/197\right)^{1/4} \; 984/f \quad , \tag{13}$$

where

D is the diameter in inches (1 in. = 25.4 mm),
f is the antenna's center frequency in MHz, and
R_r is the antenna radiation resistance, chosen to be 50 ohms.

This equation applies to a loop with constant in-phase currents about its circumference.

Eight equally spaced capacitors are inserted in series with the loop. These capacitors both tune the loop to resonance and insure uniform current around the loop. The antenna could be fed across any of these capacitors, but since an unbalanced feed line is desired, a different technique is used.

A balanced loop can be bisected by a ground plane without the loop characteristics being upset. Each half of the loop can be driven from an unbalanced line from within the ground plane in such a manner as to produce an in-phase current around the loop. Under these conditions each feed-point impedance is 25 ohms. By use of quarter-wave matching sections of 50-ohm characteristic impedance, each feed-point impedance can be transformed to 100 ohms and these terminals connected in parallel, making a 50-ohm feed point for the system, as shown in figure 4. The location of the unbalanced feed point is along the axis of the loop and, hence, in the null of the antenna radiation pattern. Some residual electrical unbalance will still exist because of capacitive currents from the high side of each feed point back to the ground plane. By extending the ground plane symmetrically for some distance in the direction away from the feed, this unbalance is minimized. Figure 5 shows one of these standard antennas. Patterns and gain of these units are discussed in appendices A and B.

[2] *J. D. Kraus, Antennas, McGraw Hill (1950).*

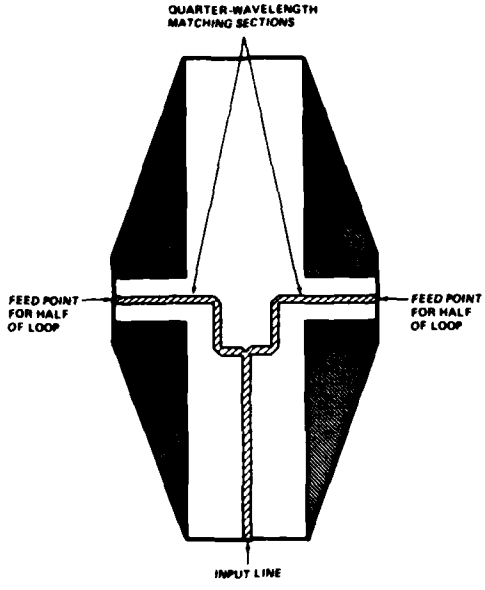

Figure 4. Antenna transmission-line configuration, strip line construction.

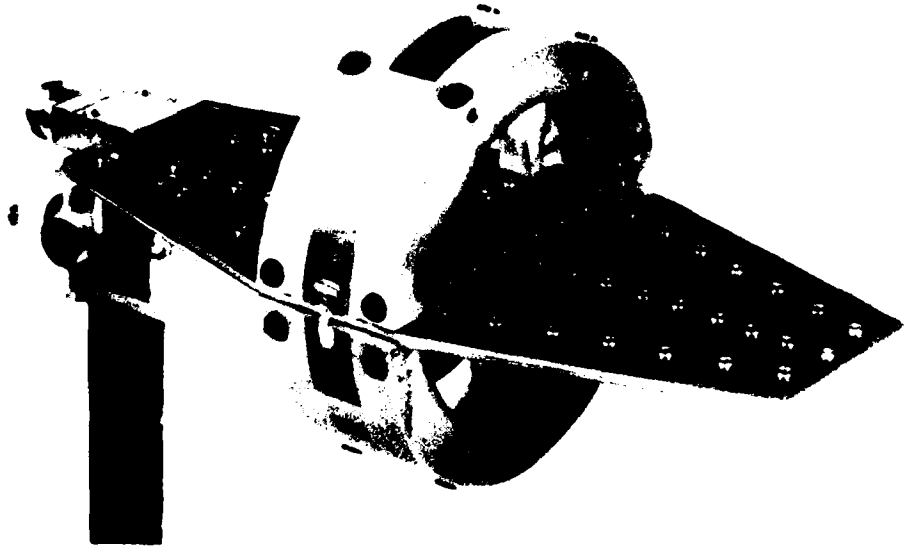

Figure 5. Antenna assembly.

4. SMALL ANECHOIC CHAMBER MEASUREMENT

The simple chamber studied in this program is shown in figure 6. The chamber is assembled with 12 sheets of 10 × 61 × 61 cm flat absorbing material. The sheets are supported by an external plywood structure not shown in the figure. One sheet near the test location is removable so that the fuze under test can be easily changed. Access ports are provided to mount the test antennas in the locations shown in figure 7. The test antennas are fixed in place and need no adjustments. The fixed position for the fuze under test is designed so that the standard antenna can be placed in the same location when necessary.

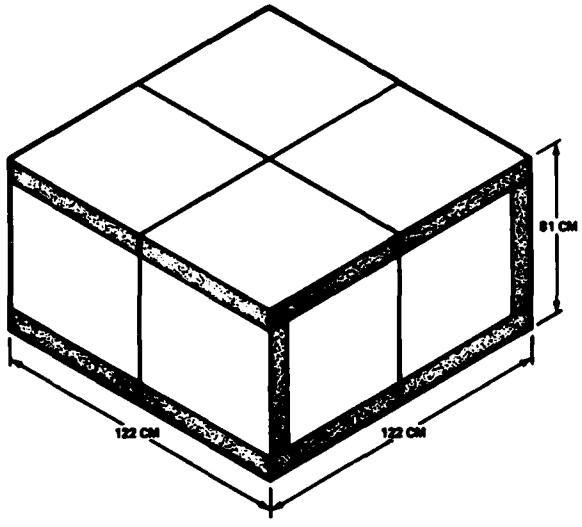

Figure 6. Small anechoic test chamber.

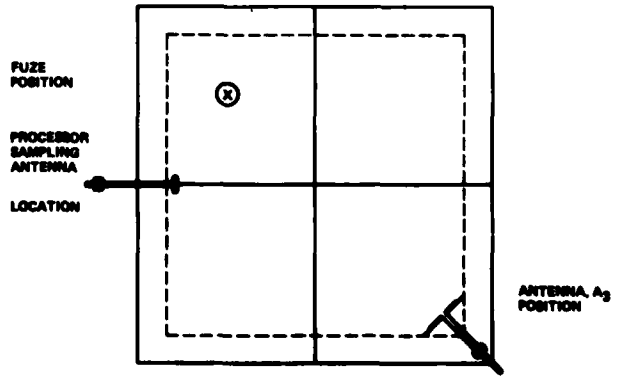

Figure 7. Antenna and fuze test positions.

The small chamber used in this test was not rf shielded, but shielding is desirable when the chamber is surrounded by strong external fields. The shielding further isolates the fuze under test from external influence.

Several types of measurements were performed to determine the relative performance of the small chamber and a large anechoic chamber (7.62 × 7.62 × 15.24 m). The tests were as follows: first, two antennas were placed in the small chamber on a diagonal line parallel to the top and bottom and passing through the center of the chamber, as shown in figure 7. Insertion loss measurements were performed for various antenna locations at several frequencies: 600, 700, 800, 900, and 1000 MHz. These data can be compared to similar data taken in the large anechoic chamber. In addition, sensitivity measurements were made on 40 fuzes in both chambers. These same fuzes had previously been measured on pole tests.

Figure 8 is the small chamber data for different spacing between the test antennas A_2 and A_3; A_3 was fixed and A_2 moved. Similar data for the large anechoic chamber are shown in figure 9 but only at a single frequency.

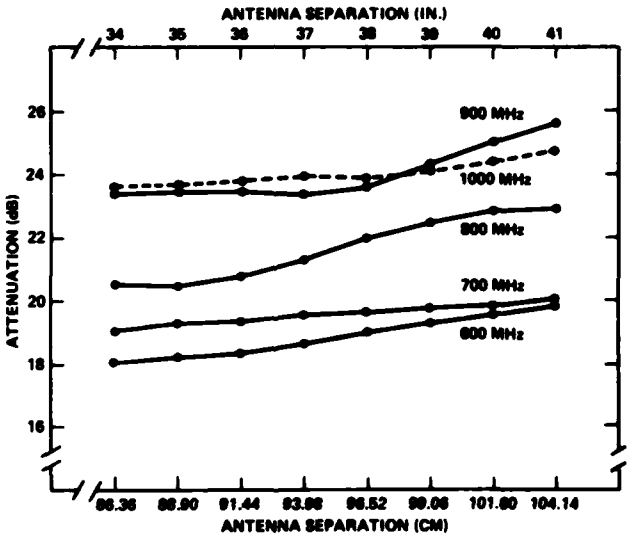

Figure 8. Small anechoic chamber: matched attenuation versus antenna spacing.

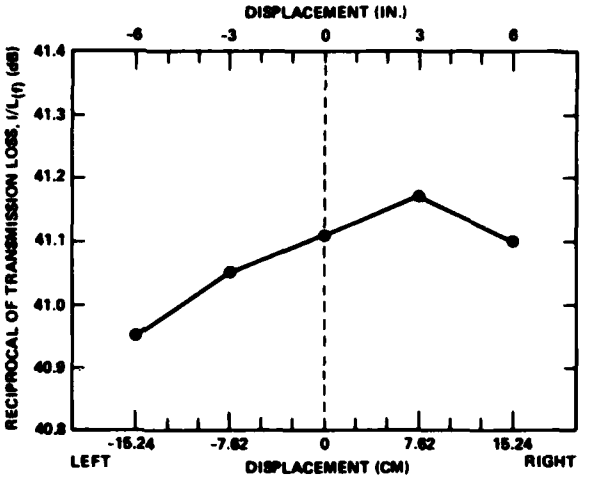

Figure 9. Large anechoic chamber: reciprocal loss (1L/(f)) for axial displacements.

In figure 10, the transverse locaton of A_2 was changed for a fixed antenna spacing. These plots indicate the changes in attenuation that can be expected for different locations of antenna A_2. From these data, a fuze mounting location is selected which will minimize the change in attenuation with respect to position, thus minimizing the error in measuring fuze sensitivity resulting from small errors in placement of the fuze in the chamber. Once a position is chosen, a mechanical mount can be assembled which will assure that the fuze under test and antenna A_2 are in the same location. Similar attenuation data for transverse position obtained for the large anechoic chamber are presented in figure 11.

Figure 12 is the precalibration curve for the small chamber, showing 1/L(f) versus frequency. This plot is obtained by performing loss measurements using antennas A_2 and A_3 with A_2 in the place where the fuze is during the sensitivity measurement. This plot was obtained by using each standard antenna over its useful range.

Fuze sensitivity measured in the small chamber was then compared with that measured in the large chamber. Two separate sets of test data were obtained for each of 40 fuzes in each chamber. The first set of measurements was taken after chamber calibration. The fuzes were remeasured after the test fixture was removed and repositioned as well as possible in the chamber, but without recalibration. Correlation plots were then made by plotting one set of data against the other.

These correlation plots are shown in figures 13, 14, and 15. The same fuzes were also measured twice on a preferred pole-test facility of an HDL contractor. This facility had in the past produced the greatest degree of repeatability. Figures 16, 17, and 18 are the correlation plots for pole-test data versus pole-test data, small-chamber data versus pole-test data, and large-chamber data versus pole-test data, respectively.

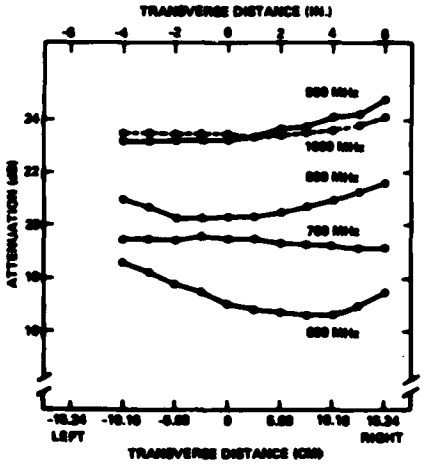

Figure 10. Small anechoic chamber: matched attenuation versus transverse displacement.

Figure 11. Large anechoic chamber: loss (1/L(f)) for transverse movement of antenna A_2.

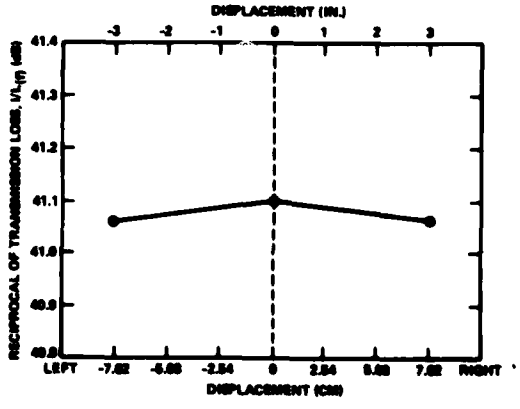

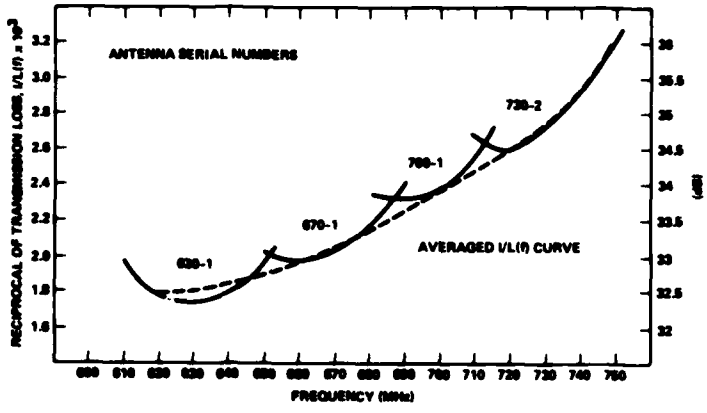

Figure 12. Small anechoic chamber calibration curve.

Figure 13. Correlation plot for two runs in small anechoic chamber.

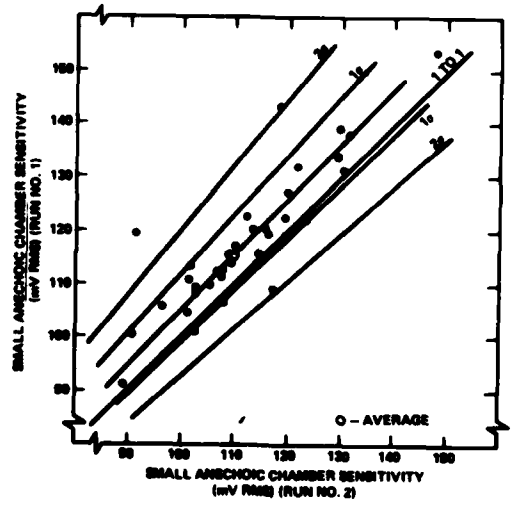

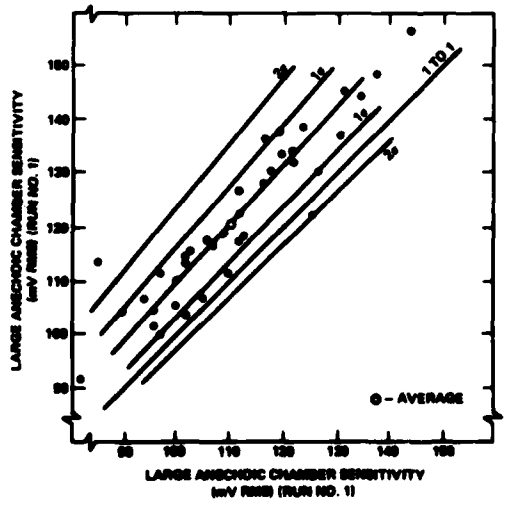

Figure 14. Correlation plot for two runs in large anechoic chamber.

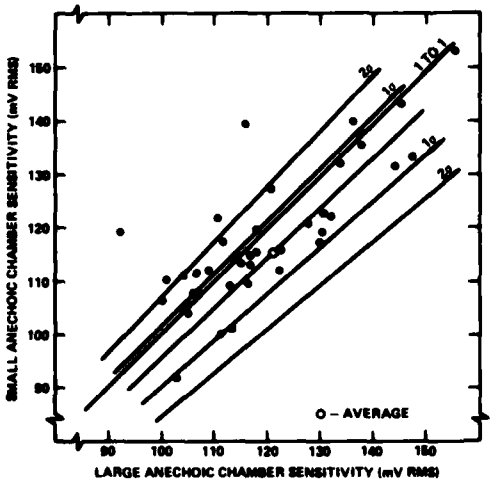

Figure 15. Correlation plot for runs in small versus large anechoic chamber.

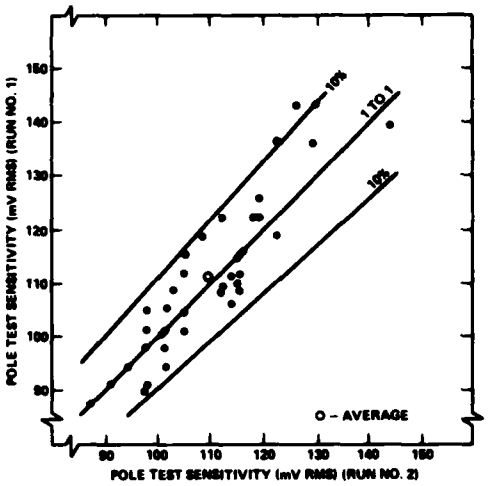

Figure 16. Correlation plot for two runs of pole test.

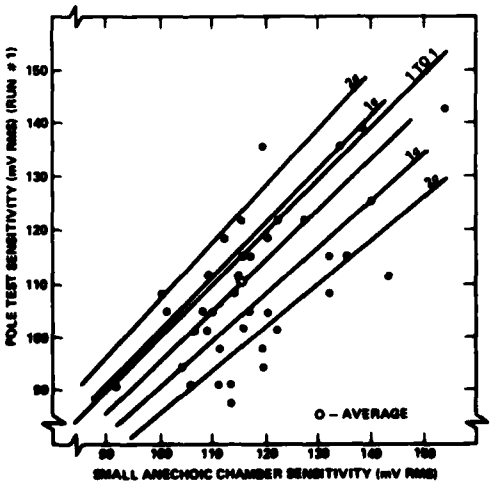

Figure 17. Correlation plot for pole test versus small anechoic chamber.

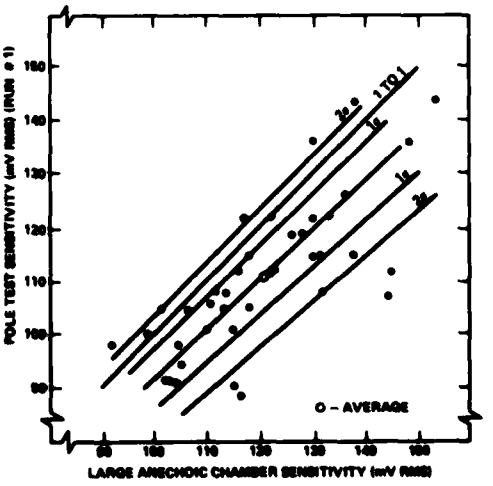

Figure 18. Correlation plot for pole test versus large anechoic chamber.

5. ERROR ANALYSIS

The accuracy of the sensitivity measurement can be estimated from figures 8, 9, 10, and 11, and from examination of equation (9). The sources of errors can be divided into three categories: antenna location and placement errors, metering equipment errors, and meter reading errors. The data in the correlation plots include all these errors. Meter reading errors can be minimized by patience and care, and certain metering equipment errors will tend to cancel as will be shown later.

A sample of 40 fuzes was tested three different ways: by a pole test (at what is considered to be the best available pole-test facility), in a large anechoic chamber (7.62 × 7.62 × 15.24 m), and in the small anechoic chamber described earlier in this report. In each of the three facilities, two sets of sensitivity measurements were performed on each fuze. In the case of the pole test, all 40 fuzes were measured once, and then the same 40 fuzes were retested on the same facility.

For the chamber measurements the test equipment was set up, and a calibration cuve (1/L(f) versus frequency) was obtained as described in section 2. The sensitivity of the 40 fuzes was then measured. Antenna positions and fuze locations were noted, and the test setup was dismantled and then reset up for a second test. No new calibration curve was run, however. An error may, thus, be introduced by not using the same mean distance between A_3 and the fuzes under test. Several other sources of error are possible (for example, temperature effects and fuze power supply variations), but care was taken to minimize variations in these quantities.

All sensitivity data calculated for the chamber tests used the same fixed value of antenna gain, 1.22, regardless of frequency. The estimated accuracy with which the gain was known at the various frequencies did not seem to justify using a different gain for each frequency. Since the antenna gain varies over any given antenna bandwidth, and the antenna gain was included while the 1/L(f) plots were obtained, a smoothed curve was used in the sensitivity calculations along with the constant antenna gain value of 1.22. The small anechoic chamber smoothed curve is shown in figure 12.

In the case of the small chamber, the random errors can be estimated from information in figures 8 and 10. Typically, the attenuation varies about 0.16 dB/cm for either transverse, lateral, or vertical displacements of the fuze from the calibration position. The estimated transverse and lateral displacement error is on the order of 0.635 cm each. Possible vertical displacement is on the order of 0.254 cm. The estimated rms error due to these factors alone is 3.5 percent. The

remaining random errors occur in measuring P_j, P_f, and E_m of equation (9). Assuming that meter reading errors on the order of 1 percent are typical, then the rms error contributed by reading these quantities is 1.2 percent. The total random error is then 3.8 percent.

The large-chamber random errors are comparable to those in the small chamber, since our ability to relocate the antenna and fuze positions exactly is estimated to have a larger absolute error.

The estimated random error of 3.8 percent leads to a scattering of the data points in the correlation plot. We may analyze this as follows: Consider the i^{th} fuze of a sample of n fuzes where actual but unknown sensitivity is S_0^i. In the correlation plot one measurement of a fuze is plotted against the second measurement of the same fuze. Each measurement is independent and subject to random errors defined by a σ of 3.8 percent, assuming the errors to be Gaussian. We may depict this pair of measurements on the i^{th} fuze by the point X^i in figure 19. The error δ_1^i was associated with the first measurement and δ_2^i with the second. Thus,

$$\varepsilon_1^i = \frac{\delta_1^i}{S_0^i} \quad , \tag{14}$$

$$\varepsilon_2^i = \frac{\delta_2^i}{S_0^i} \quad , \tag{15}$$

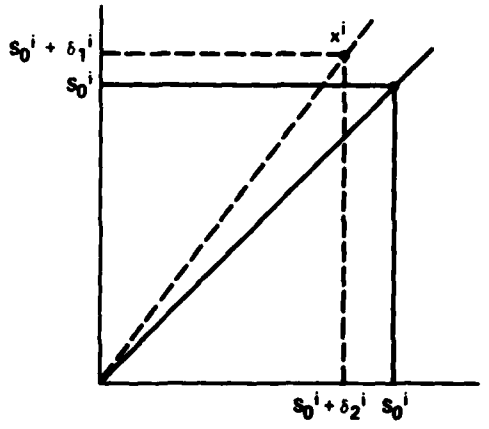

Figure 19. Sample correlation plots depicting errors.

where ε_1 and ε_2 are the per unit errors associated with each measurement. For each fuze, then, there will be a different point X^i and slope M^i defined by

$$M^i = \frac{1 + \varepsilon_1^i}{1 + \varepsilon_2^i} \quad . \tag{16}$$

Expanding the denominator in a power series and keeping only the first-order terms gives

$$M^i = \left(1 + \varepsilon_1^i\right)\left(1 - \varepsilon_2^i\right) \quad , \tag{17}$$

or

$$M^i = 1 + \varepsilon_1^i - \varepsilon_2^i - \varepsilon_1^i\varepsilon_2^i \quad . \tag{18}$$

Again dropping second-order terms gives

$$M^i = 1 + \varepsilon_1^i - \varepsilon_2^i \quad . \tag{19}$$

The mean value of the slope for n fuzes is then

$$\begin{aligned} \overline{M^i} &= \frac{1}{n} \sum_{i=1}^{n} 1 + \left(\varepsilon_1^i - \varepsilon_2^i\right) \\ &= 1 + \frac{1}{n} \sum_{i=1}^{n} \varepsilon_1^i - \frac{1}{n} \sum_{i=1}^{n} \varepsilon_2^i \quad , \end{aligned} \tag{20}$$

or

$$\overline{M^i} = 1 \quad , \tag{21}$$

since

$$\sum_{i=1}^{n} \varepsilon_K^i = 0 \quad .$$

If we were to form a frequency histogram of slope versus slope for a fuze sample of n fuzes, we would expect to approximate a Gaussian density function p(m) (fig. 20).

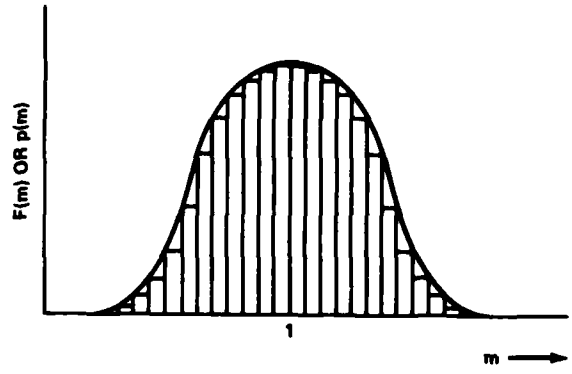

Figure 20. Frequency histogram of p(m) versus m.

Since each point X^i with slope m^i represents one fuze, one can count the number of fuzes falling within the ±1σ or ±2σ limits of F(m). The standard deviation of the slopes can be found as follows:

$$\sigma^2 = \left(m^i - m_i\right)^2 = \left(\varepsilon_1^i - \varepsilon_2^i\right)^2$$

$$= \frac{1}{n} \sum_{i=1}^{n} \left[\left(\varepsilon_1^i\right)^2 + \left(\varepsilon_2^i\right)^2 - 2\varepsilon_1^i\varepsilon_2^i\right] \quad , \tag{22}$$

where

$$\frac{2}{n} \sum_{i=1}^{n} \varepsilon_1^i\varepsilon_2^i = 0 \quad .$$

Since ε_1^i and ε_2^i are independent, therefore,

$$\sigma^2 = \frac{1}{n} \sum_{i=1}^{n} \left(\varepsilon_1^i\right)^2 + \frac{1}{n} \sum_{i=1}^{n} \left(\varepsilon_2^i\right)^2 \quad ,$$

or

$$\sigma^2 = \sigma_1^2 + \sigma_2^2 \quad . \tag{23}$$

Assuming $\sigma_1 = \sigma_2 = 0.038$, as estimated earlier, $\sigma = 0.054$. If there is no fixed bias between the two sets of measurements, 68 percent of the samples should lie within ±5.4 percent, and 95 percent within ±10.8 percent of unit slope.

Small anechoic chamber correlation plot (fig. 13).--Two sensitivity measurements were run as previously described. The plot indicated a fixed-point bias error of approximately 4.2 percent, as noted by the

location of the average point (x) with respect to the one-to-one line. Of the data points 86 percent lie within the 1σ lines and 95 percent lie within the 2σ lines. No doubt a major portion of the 4.2-percent bias error is due to a change in the mean distance between the fuze and antenna A_3.

Large anechoic chamber correlation plot (fig. 14).--This plot shows a fixed bias error of approximately 9 percent between the average correlation point (x) and the one-to-one line. Most of this error is probably due to the location of the fuze with respect to the calibration position of antenna A_2. Of the data points 82 percent lie within the 1σ lines and 97 percent lie within the 2σ lines.

Small-chamber/large-chamber correlation plot (fig. 15).--These two sets of data points have a bias error of 4 percent. Of the data points, 61 percent lie within the 1σ lines and 90 percent lie within the 2σ lines.

Pole-test correlation plot (fig. 16).--The estimate of the errors in this correlation plot can only be the random error since no other data are available. Of the data points, 95 percent lie within the 10-percent lines with the average correlation point (x) lying near the one-to-one line.

Pole-test/chamber correlation plots (fig. 17 and 18).--Both correlation plots show approximately the same results. Both plots have approximately the same average correlation point (x) which lies at the 5-percent line for the small chamber and at the 10-percent line for the large chamber, the chambers yielding the larger sensitivity magnitudes. The data point spread is larger than the previous correlation plots, which one could expect from independent tests.

The remaining errors in the equation involve two parameters, the previously determined errors and the antenna A_2 gain, G_2. The largest single error is associated with the measurement of the antenna gain, G_2, and is the error most difficult to determine. The antenna gain error was determined by the National Bureau of Standards (NBS) during the gain measurements that they performed. Data are presented in appendix B. Using the NBS quadrature sum error of 0.4 dB, or 0.097 for the antenna gain, and 0.038 from the previous analysis results in an overall estimated error of 0.104 or 10.4 percent.

6. CONCLUSION

Production-line fuze testing can be performed in a small anechoic chamber using the oscillator sensitivity measurement technique. The chamber is premeasured for system loss versus frequency; by using the data and by performing two power measurements, one frequency measurement, and a detector voltage measurement, both sensitivity and radiated power can easily be calculated.

A desirable feature of any chamber employed for this sensitivity measuring technique is shielding from external fields. The shielding is accomplished by constructing the chamber wall with one or two layers of a continuous metal surface.

The calculated overall system error of the small anechoic chamber measuring system is 10.4 percent. Careful relative positioning of the fuze and antenna A_2 and the location of antenna A_3 is important in reducing measurement error. This was illustrated in this report by the correlation tests run for small-chamber versus small-chamber data, and the large-chamber versus large-chamber data where the test equipment is torn down between tests.

APPENDIX A.--LOOP STANDARD ANTENNA MEASUREMENTS

CONTENTS

FIGURES (Cont'd)

APPENDIX A.--LOOP STANDARD ANTENNA MEASUREMENTS

Measurements were performed to determine the characteristics of the loop standard antenna. Two types of measurements are documented in this appendix: terminal admittance and radiation patterns. The terminal admittance data were obtained using a small anechoic chamber and a General Rodin uhf admittance meter. The obtained data were plotted on a Smith chart to determine each loop antenna's resonant frequency, admittance, and the voltage standing wave ratio (VSWR) versus frequency. From the VSWR plots, three frequencies were determined at which antenna radiation patterns were measured. These antenna measurements were performed in HDL's anechoic chamber.

The data for each of eight antennas are arranged in groups of five figures. Each group is labeled with a common antenna number (i.e., 630-1, 670-1, etc). The figures of each group are arranged in the order of two admittance plots and three antenna pattern composite plots taken at different frequencies.

The admittance measurements were taken at the frequencies indicated on the "Meter Reading" curve. The Smith chart was used, in three steps, to transform the admittance and to determine the admittance at the loop antenna feed point, labeled "Transformed by L_2." From this chart the 2:1 VSWR frequencies were determined, and composite antenna patterns were measured for the center frequency and both 2:1 VSWR frequencies.

Each antenna pattern composite figure includes data for both horizontal and vertical polarization as well as cross polarization. The chart included in each figure specifies both the test loop and reference dipole polarization used in the antenna measurements as well as the resulting patterns.

APPENDIX A

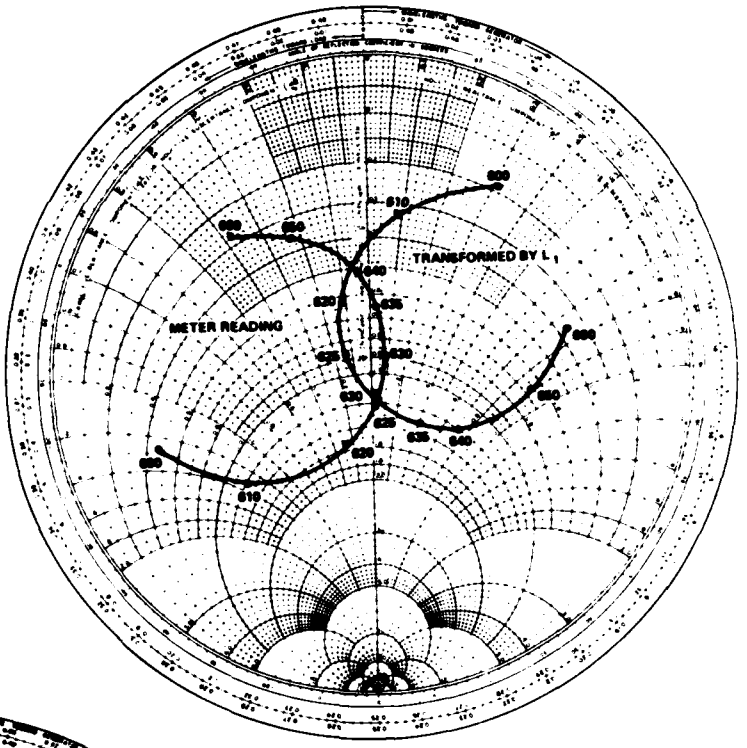

Figure A-1. Loop antenna 630-1 admittance measurements versus frequency in MHz.

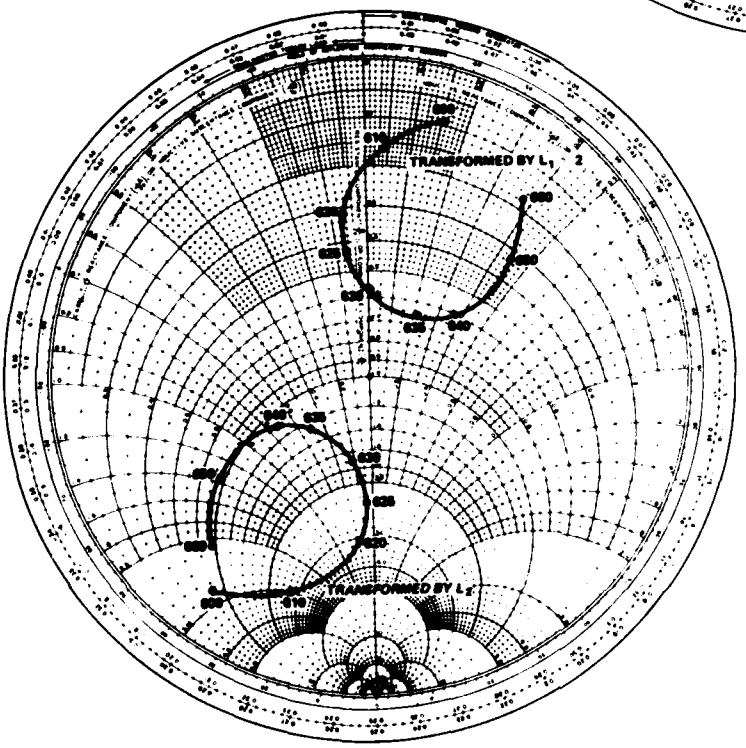

Figure A-2. Loop antenna 630-1 admittance measurements versus frequency in MHz.

Figure A-3. Loop antenna 630-1 radiation pattern measurements at 616 MHz.

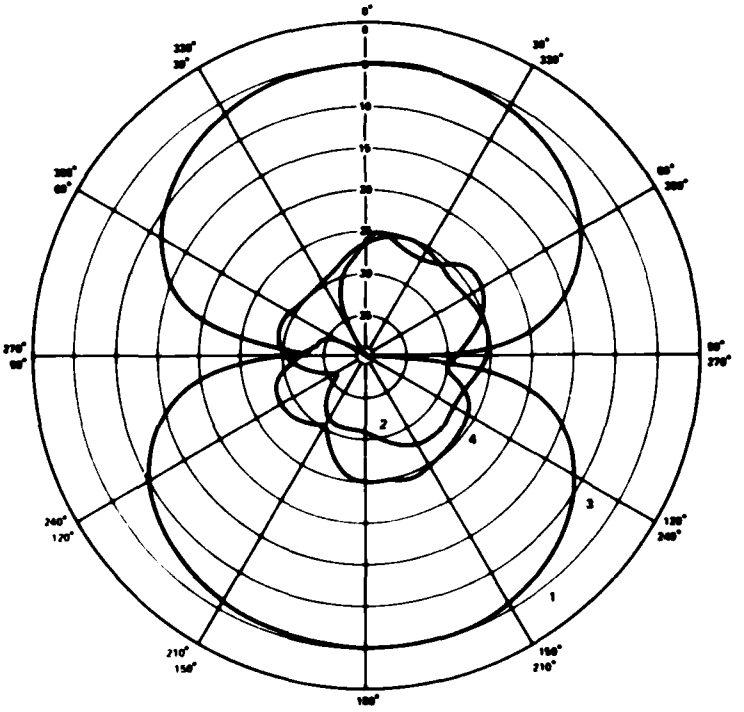

ANTENNA ORIENTATION		
TEST NO	TEST LOOP	DIPOLE
1	HORIZ	HORIZ
2	HORIZ	VERT
3	VERT	VERT
4	VERT	HORIZ

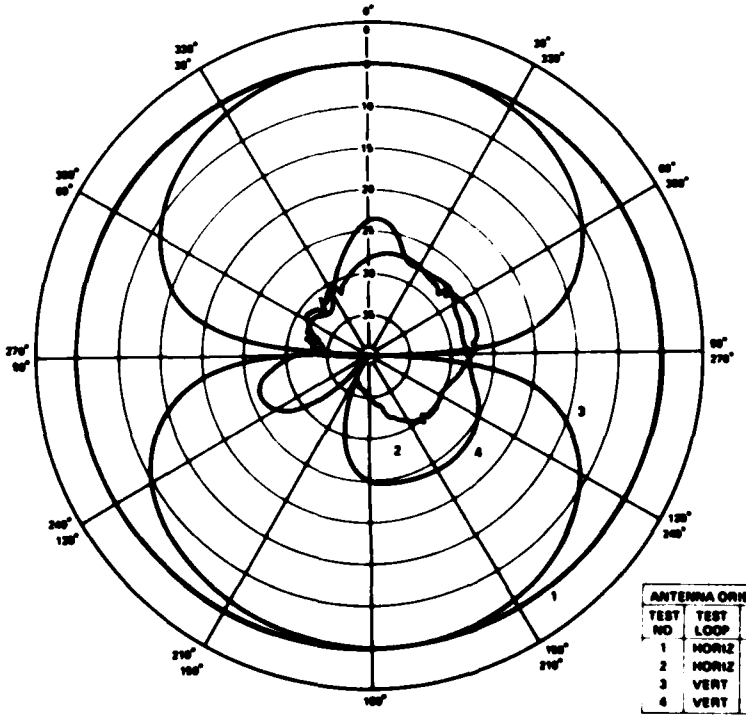

Figure A-4. Loop antenna 630-1 radiation pattern measurements at 630 MHz.

ANTENNA ORIENTATION		
TEST NO	TEST LOOP	DIPOLE
1	HORIZ	HORIZ
2	HORIZ	VERT
3	VERT	VERT
4	VERT	HORIZ

APPENDIX A

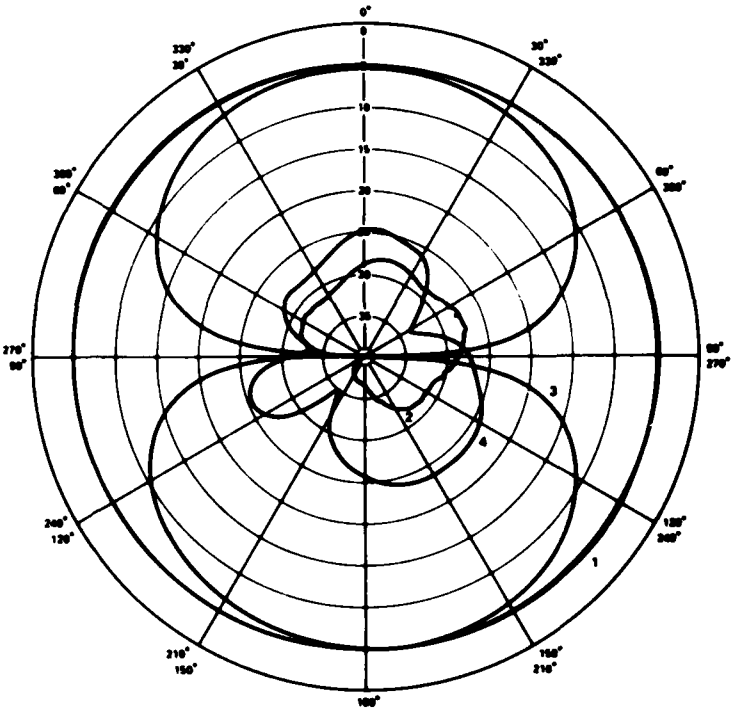

Figure A-5. Loop antenna 630-1 radiation pattern measurements at 640 MHz.

ANTENNA ORIENTATION		
TEST NO	TEST LOOP	DIPOLE
1	HORIZ	HORIZ
2	HORIZ	VERT
3	VERT	VERT
4	VERT	HORIZ

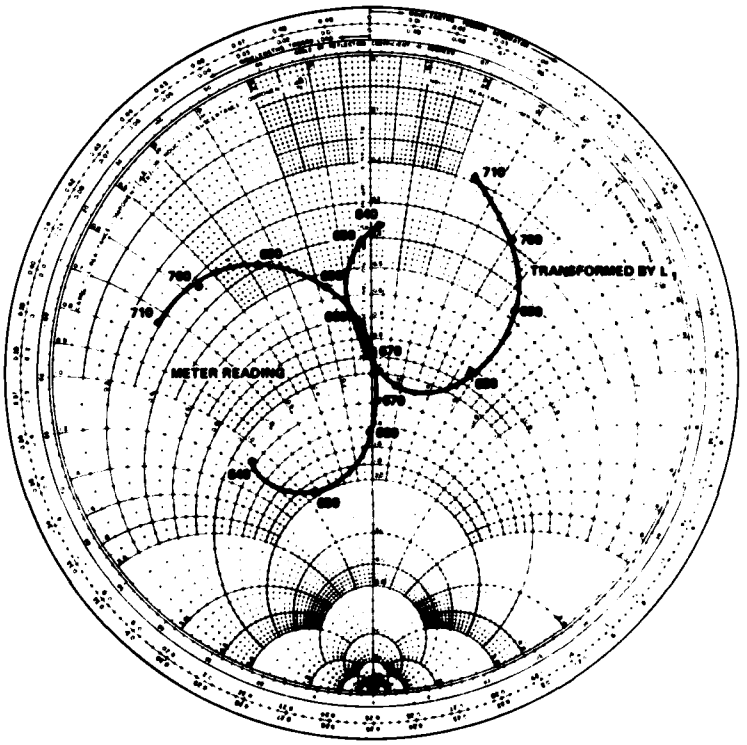

Figure A-6. Loop antenna 670-1 admittance measurements versus frequency in MHz.

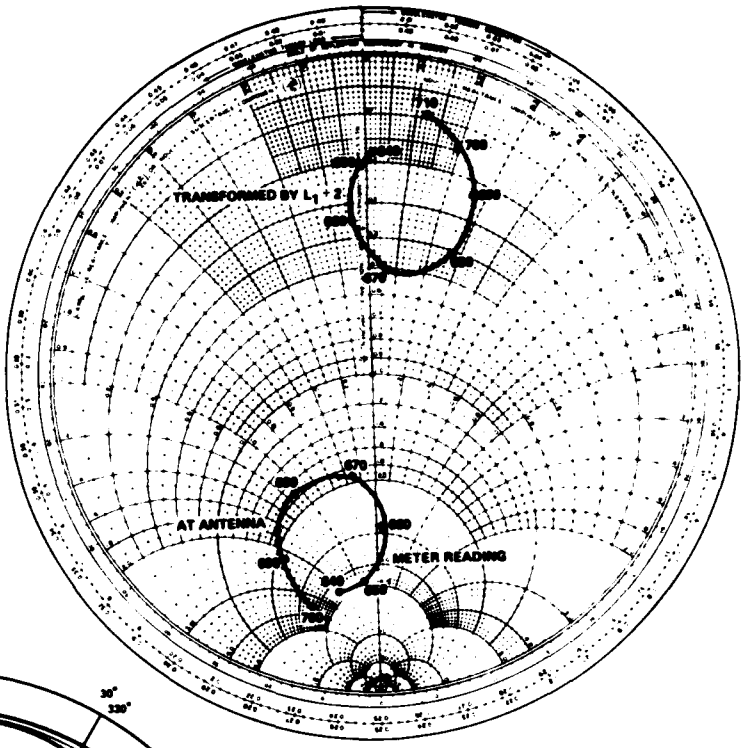

Figure A-7. Loop antenna 670-1 admittance measurements versus frequency in MHz.

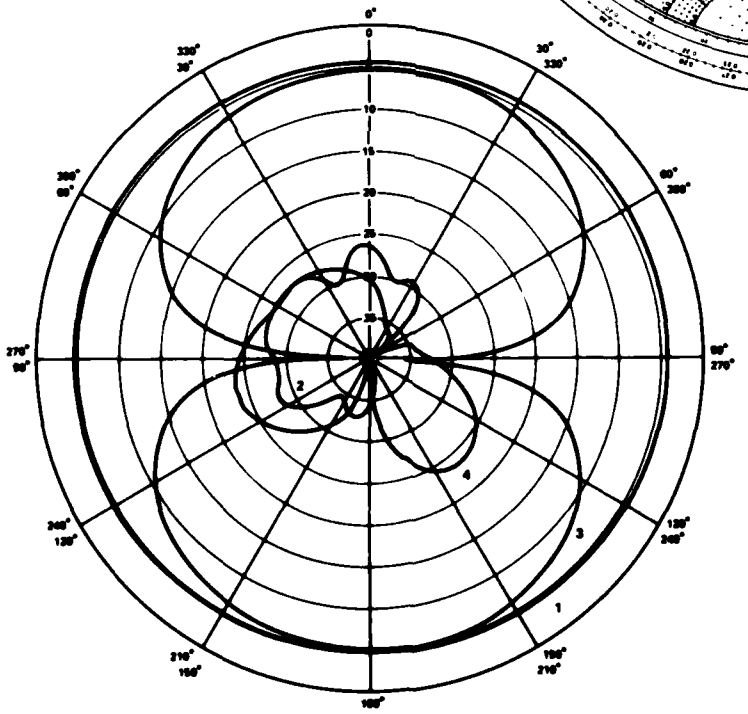

Figure A-8. Loop antenna 670-1 radiation pattern measurements at 658 MHz.

ANTENNA ORIENTATION		
TEST NO.	TEST LOOP	DIPOLE
1	HORIZ	HORIZ
2	HORIZ	VERT
3	VERT	VERT
4	VERT	HORIZ

APPENDIX A

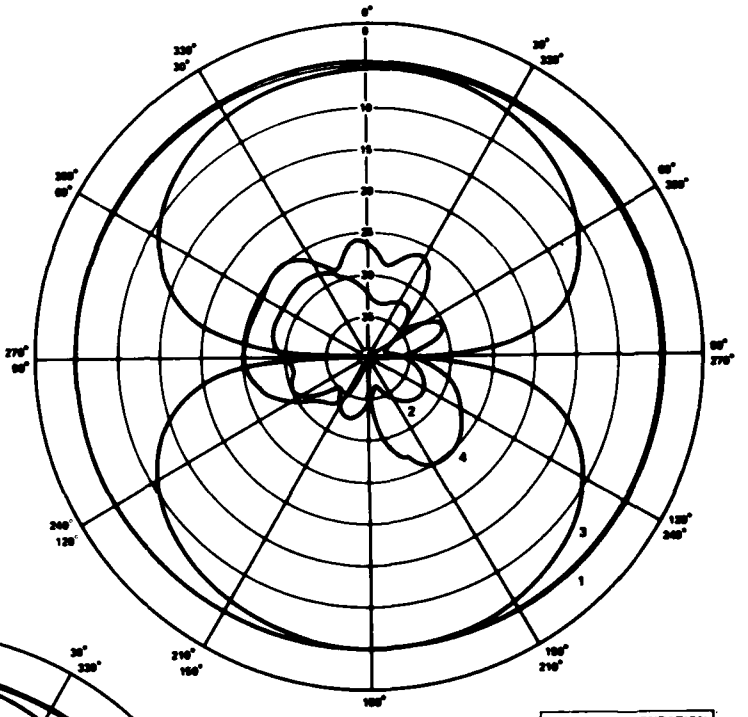

ANTENNA ORIENTATION		
TEST NO.	TEST LOOP	DIPOLE
1	HORIZ	HORIZ
2	HORIZ	VERT
3	VERT	VERT
4	VERT	HORIZ

Figure A-9. Loop antenna 670-1 radiation pattern measurements at 670 MHz.

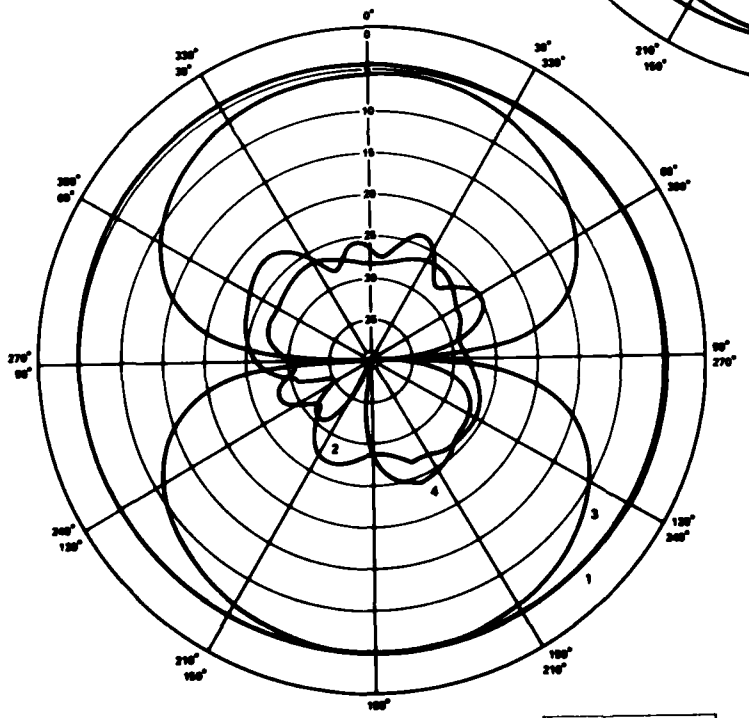

ANTENNA ORIENTATION		
TEST NO.	TEST LOOP	DIPOLE
1	HORIZ	HORIZ
2	HORIZ	VERT
3	VERT	VERT
4	VERT	HORIZ

Figure A-10. Loop antenna 670-1 radiation pattern measurements at 684 MHz.

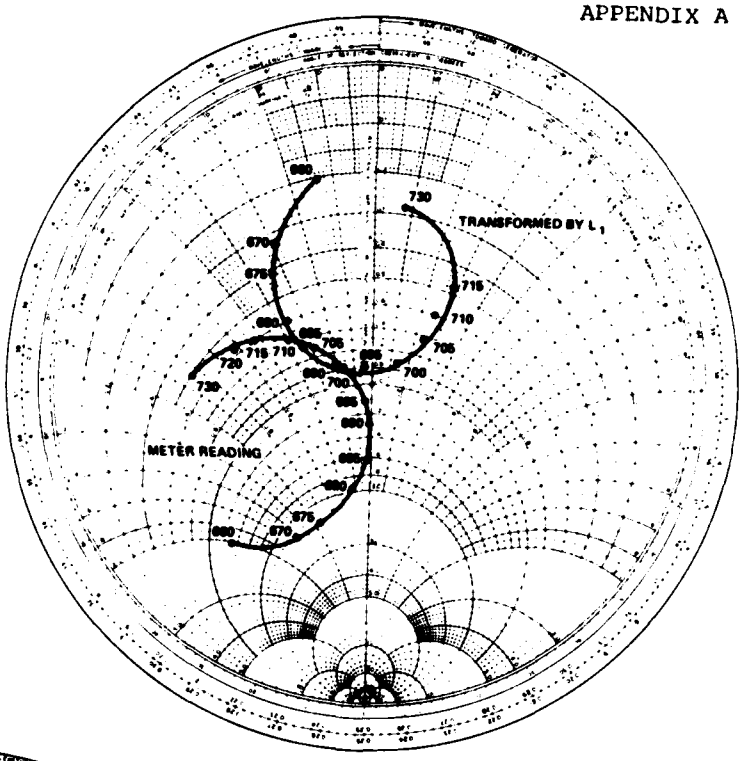

Figure A-11. Loop antenna 700-1 admittance measurements versus frequency in MHz.

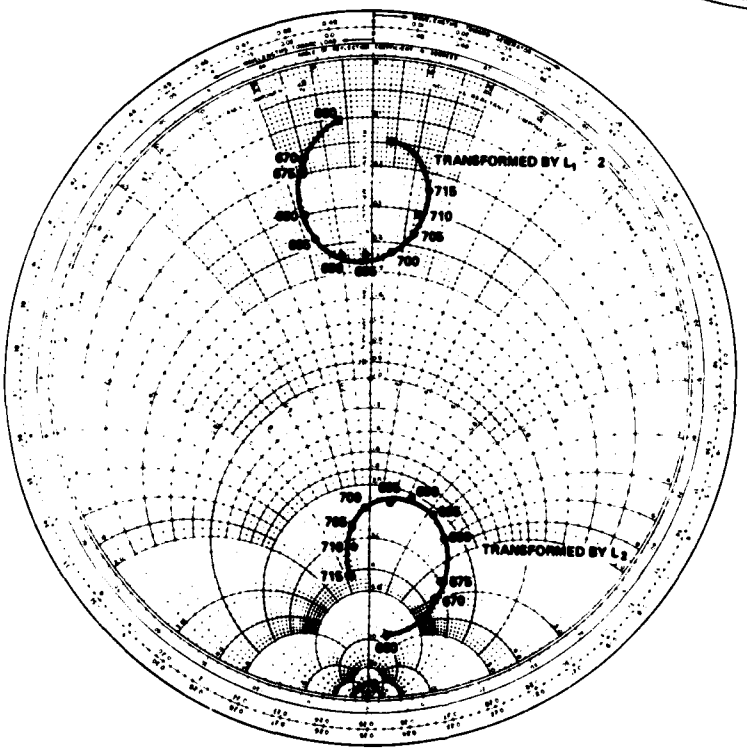

Figure A-12. Loop antenna 700-1 admittance measurements versus frequency in MHz.

APPENDIX A

Figure A-13. Loop antenna 700-1 radiation pattern measurements at 680 MHz.

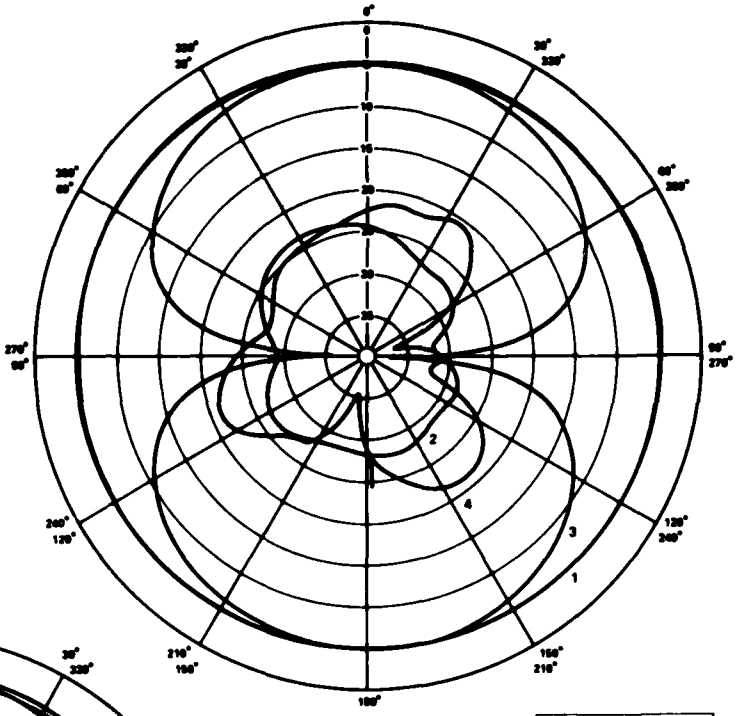

ANTENNA ORIENTATION		
TEST NO.	TEST LOOP	DIPOLE
1	HORIZ	HORIZ
2	HORIZ	VERT
3	VERT	VERT
4	VERT	HORIZ

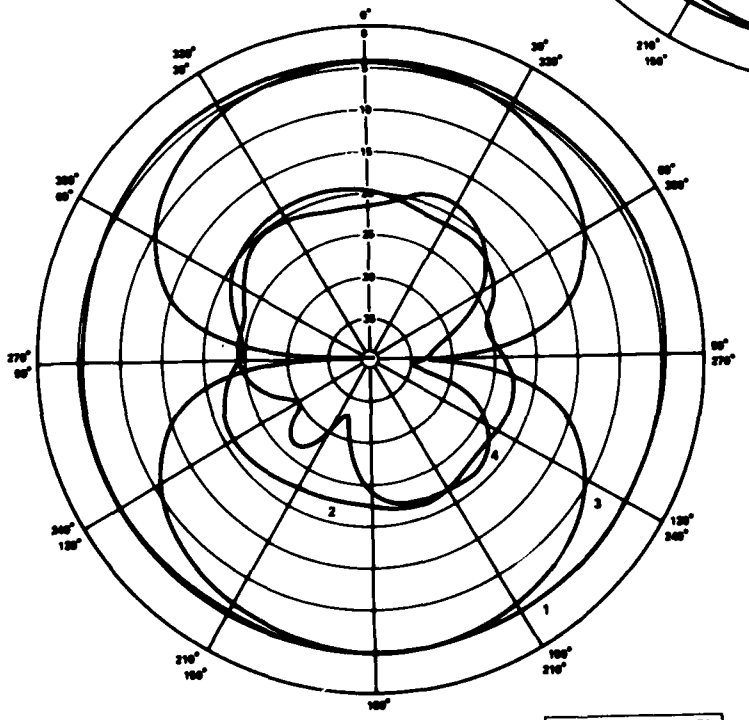

Figure A-14. Loop antenna 700-1 radiation pattern measurements at 700 MHz.

ANTENNA ORIENTATION		
TEST NO.	TEST LOOP	DIPOLE
1	HORIZ	HORIZ
2	HORIZ	VERT
3	VERT	VERT
4	VERT	HORIZ

Figure A-15. Loop antenna 700-1 radiation pattern measurements at 712 MHz.

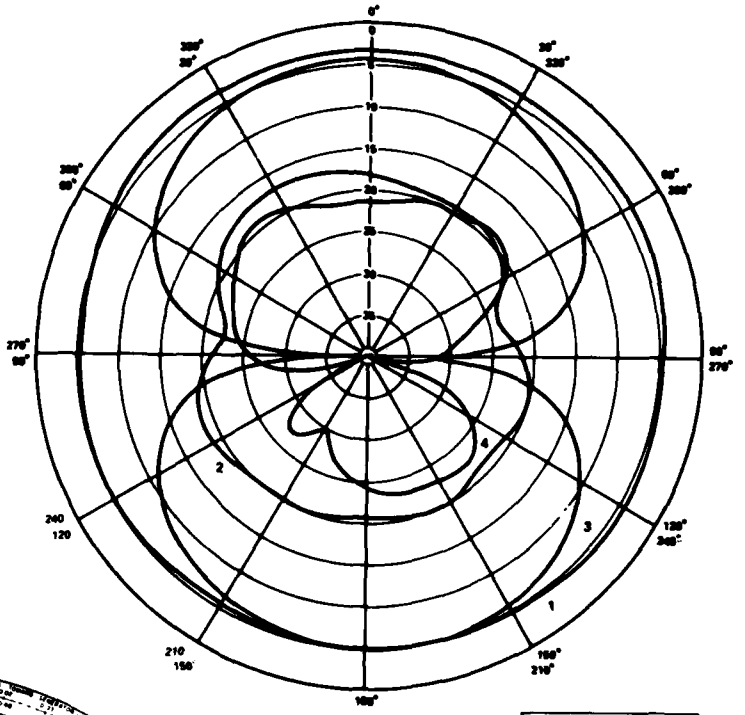

ANTENNA ORIENTATION		
TEST NO.	TEST LOOP	DIPOLE
1	HORIZ	HORIZ
2	HORIZ	VERT
3	VERT	VERT
4	VERT	HORIZ

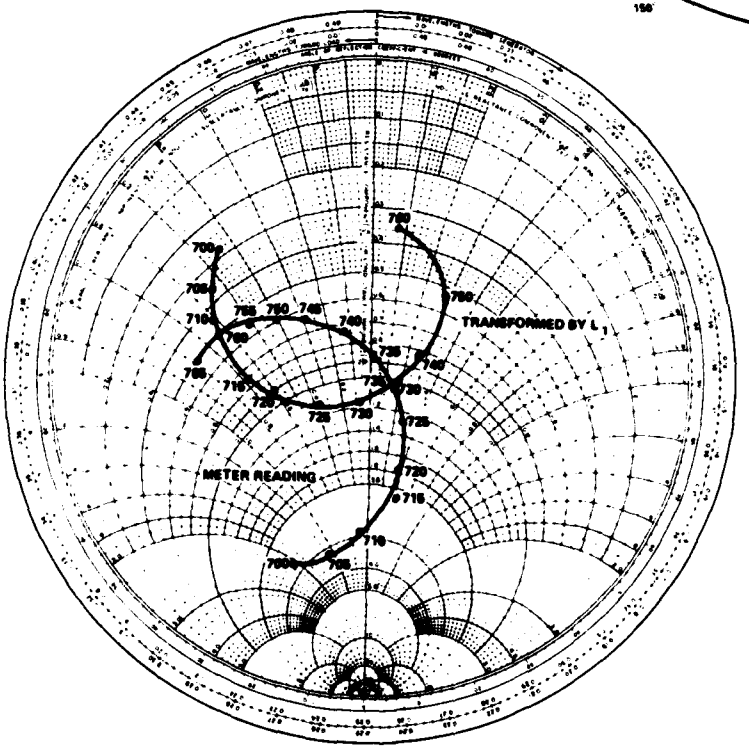

Figure A-16. Loop antenna 735-1 admittance measurements versus frequency in MHz.

APPENDIX A

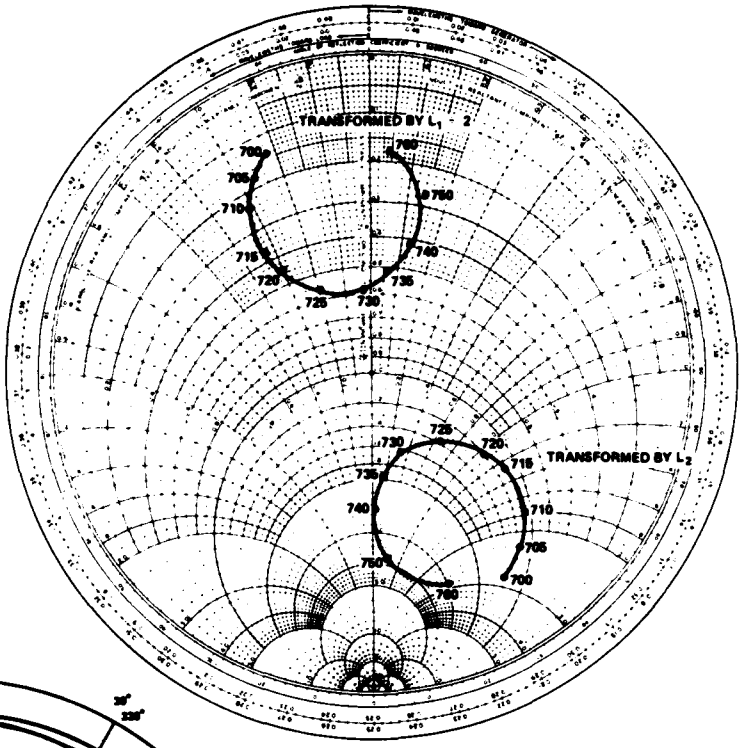

Figure A-17. Loop antenna 735-1 admittance measurements versus frequency in MHz.

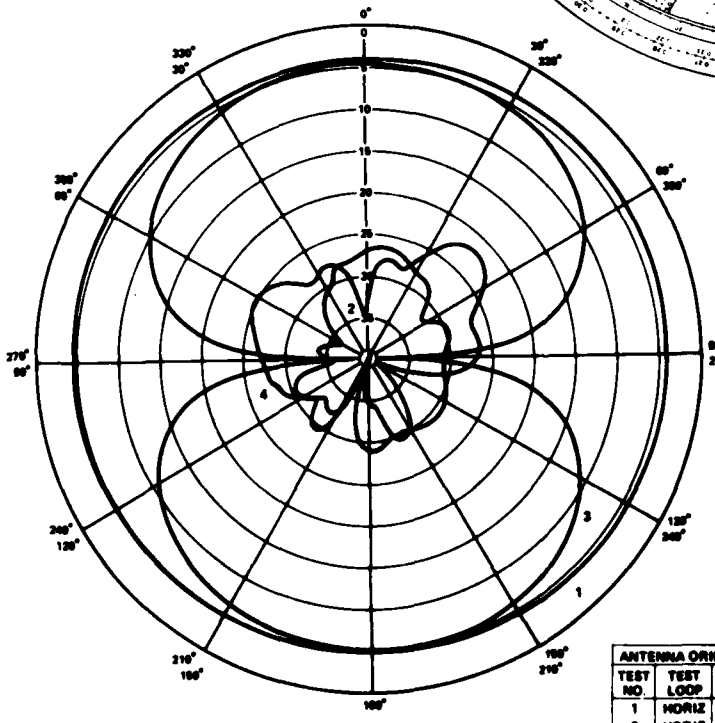

ANTENNA ORIENTATION		
TEST NO.	TEST LOOP	DIPOLE
1	HORIZ	HORIZ
2	HORIZ	VERT
3	VERT	VERT
4	VERT	HORIZ

Figure A-18. Loop antenna 735-1 radiation pattern measurements at 722 MHz.

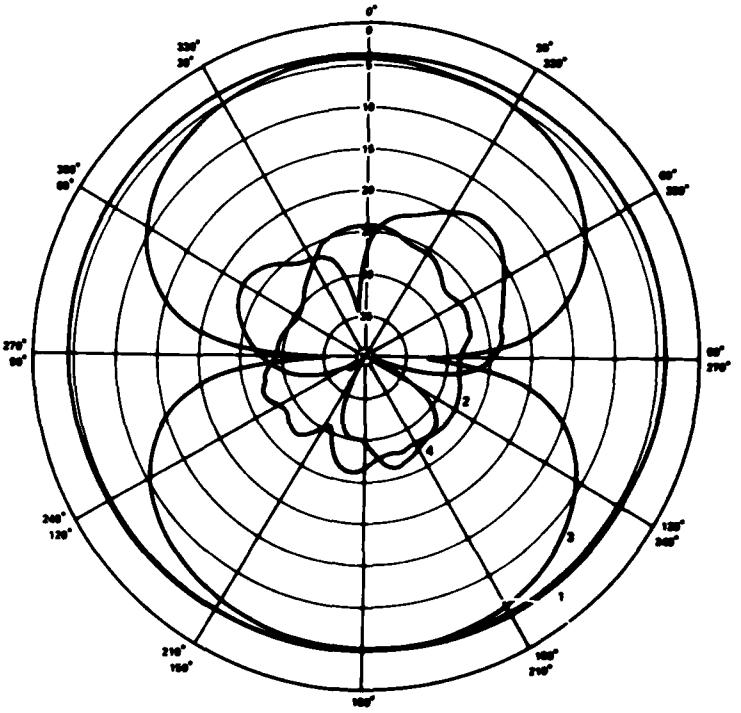

ANTENNA ORIENTATION		
TEST NO	TEST LOOP	DIPOLE
1	HORIZ	HORIZ
2	HORIZ	VERT
3	VERT	VERT
4	VERT	HORIZ

Figure A-19. Loop antenna 735-1 radiation pattern measurements at 735 MHz.

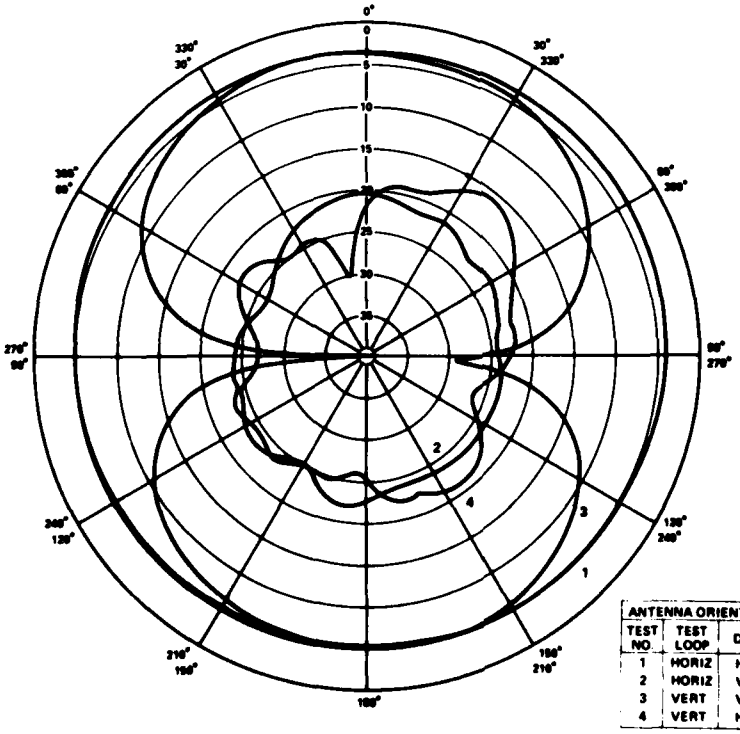

ANTENNA ORIENTATION		
TEST NO	TEST LOOP	DIPOLE
1	HORIZ	HORIZ
2	HORIZ	VERT
3	VERT	VERT
4	VERT	HORIZ

Figure A-20. Loop antenna 735-1 radiation pattern measurements at 751 MHz.

APPENDIX A

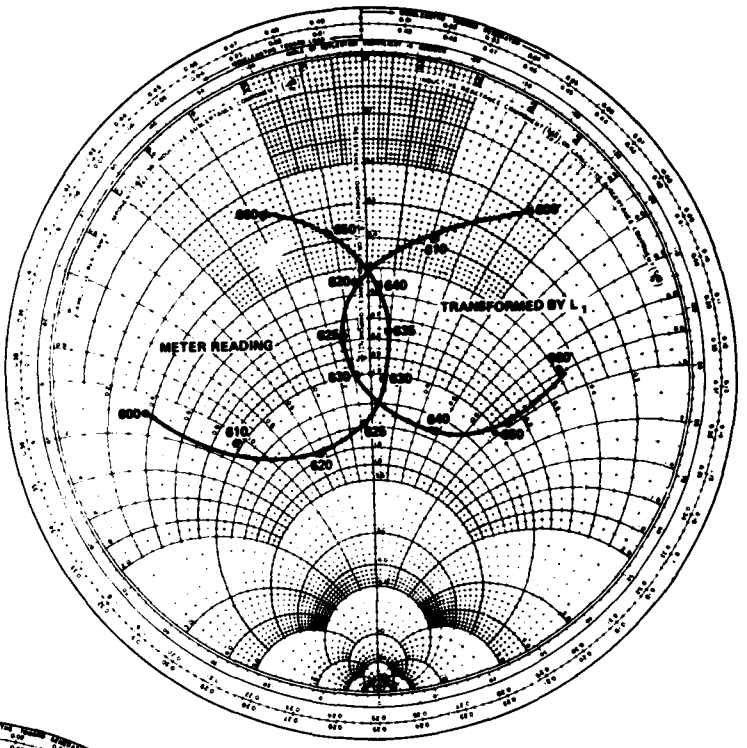

Figure A-21. Loop antenna 630-2 admittance measurements versus frequency in MHz.

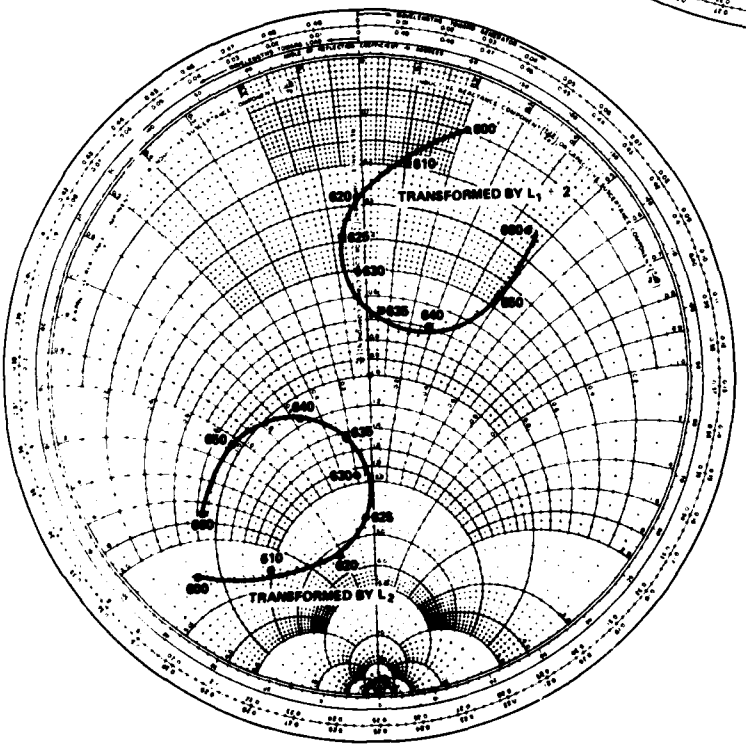

Figure A-22. Loop antenna 630-2 admittance measurements versus frequency in MHz.

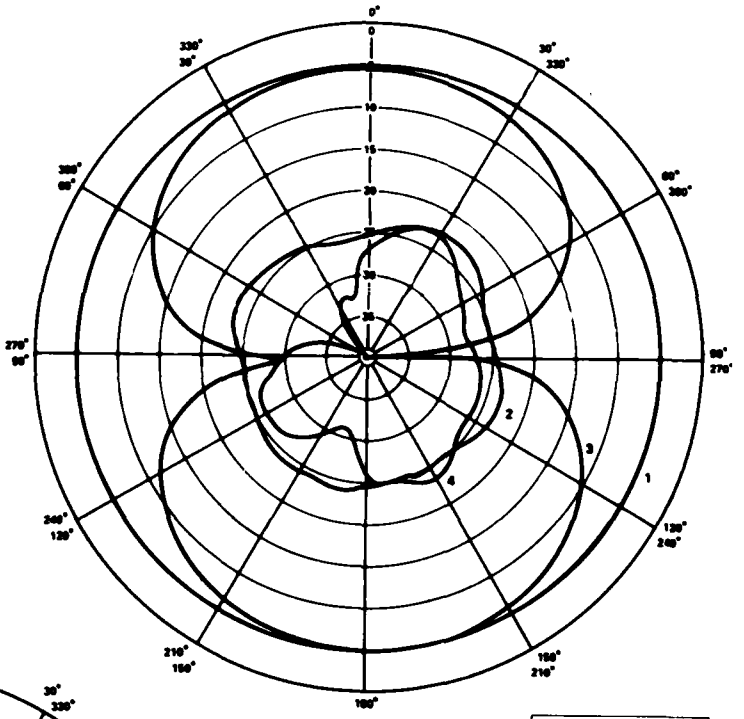

ANTENNA ORIENTATION		
TEST NO.	TEST LOOP	DIPOLE
1	HORIZ	HORIZ
2	HORIZ	VERT
3	VERT	VERT
4	VERT	HORIZ

Figure A-23. Loop antenna 630-2 radiation pattern measurements at 618 MHz.

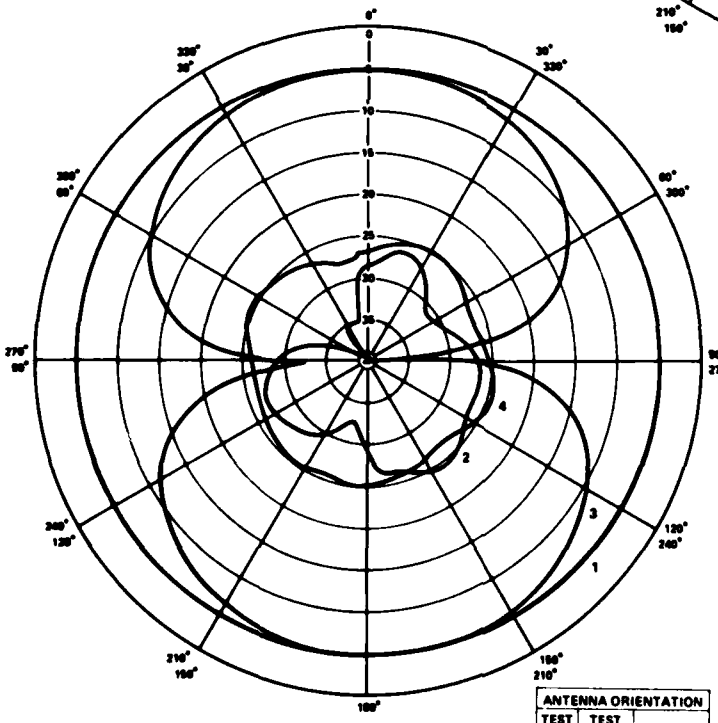

ANTENNA ORIENTATION		
TEST NO.	TEST LOOP	DIPOLE
1	HORIZ	HORIZ
2	HORIZ	VERT
3	VERT	VERT
4	VERT	HORIZ

Figure A-24. Loop antenna 630-2 radiation pattern measurements at 630 MHz.

APPENDIX A

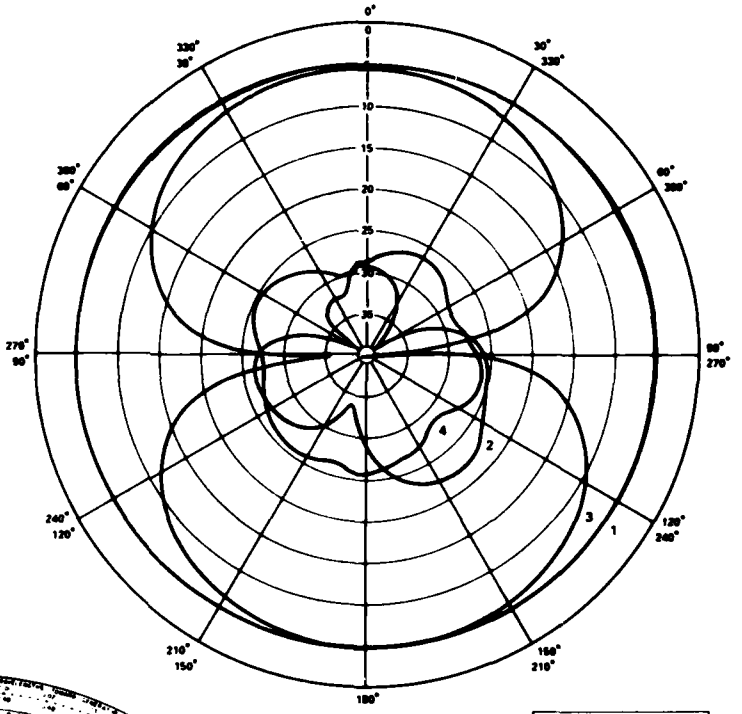

Figure A-25. Loop antenna 630-2 radiation pattern measurements at 642 MHz.

ANTENNA ORIENTATION		
TEST NO.	TEST LOOP	DIPOLE
1	HORIZ	HORIZ
2	HORIZ	VERT
3	VERT	VERT
4	VERT	HORIZ

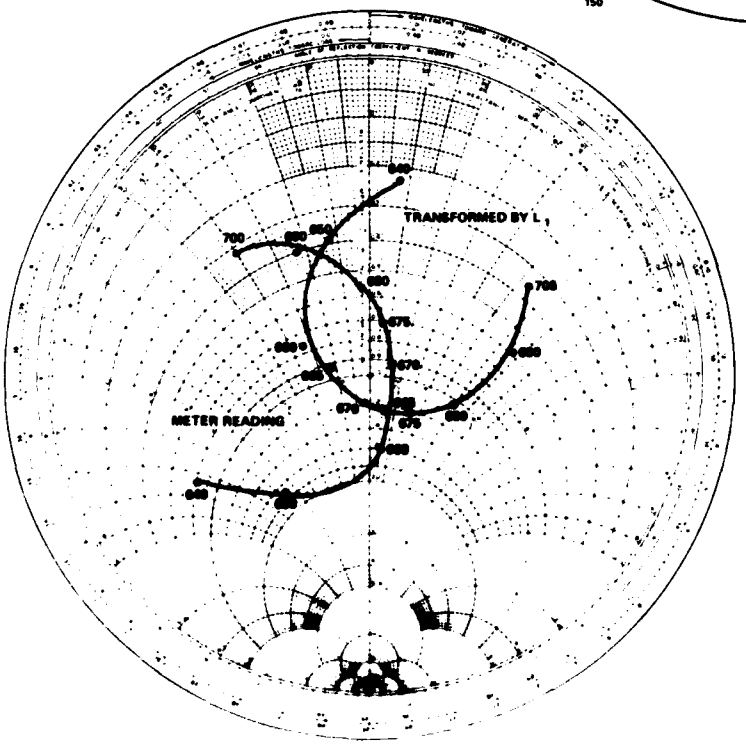

Figure A-26. Loop antenna 670-2 admittance measurements versus frequency in MHz.

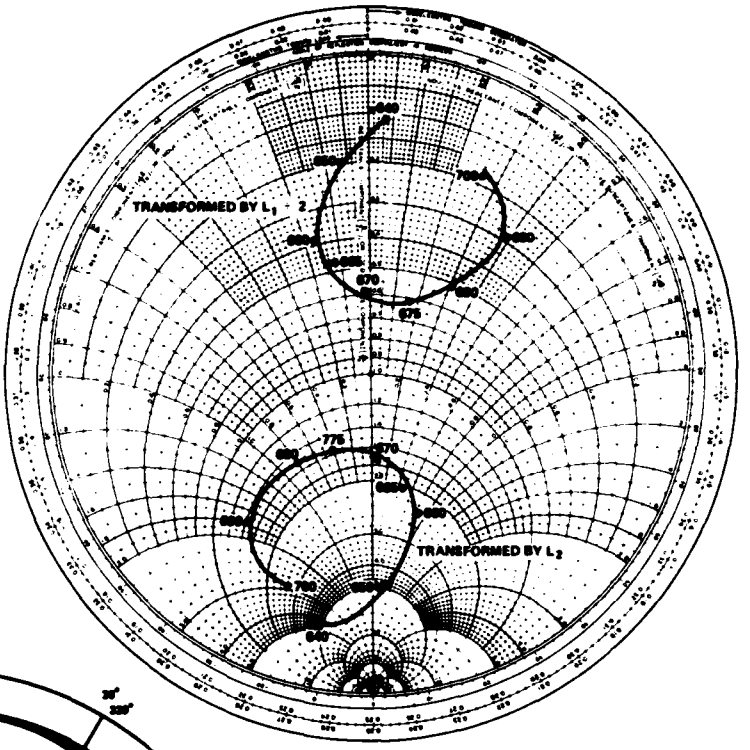

Figure A-27. Loop antenna 670-2 admittance measurements versus frequency in MHz.

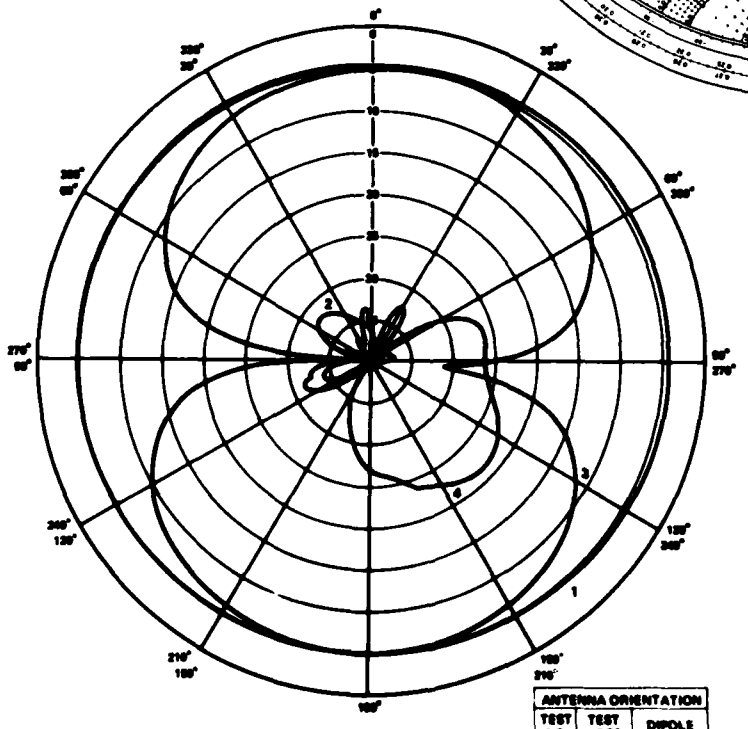

ANTENNA ORIENTATION		
TEST NO	TEST LOOP	DIPOLE
1	HORIZ	HORIZ
2	HORIZ	VERT
3	VERT	VERT
4	VERT	HORIZ

Figure A-28. Loop antenna 670-2 radiation pattern measurements at 656 MHz.

APPENDIX A

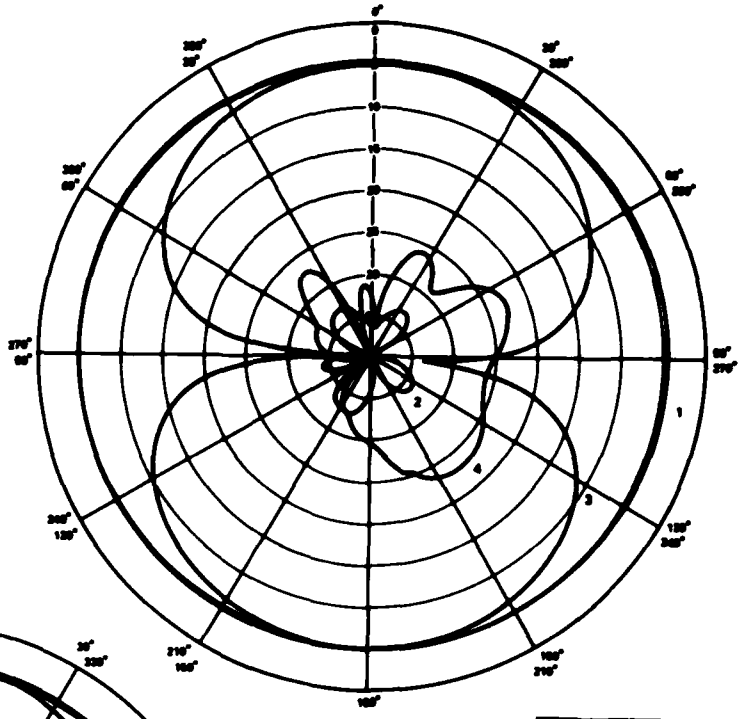

ANTENNA ORIENTATION		
TEST NO.	TEST LOOP	DIPOLE
1	HORIZ	HORIZ
2	HORIZ	VERT
3	VERT	VERT
4	VERT	HORIZ

Figure A-29. Loop antenna 670-2 radiation pattern measurements at 670 MHz.

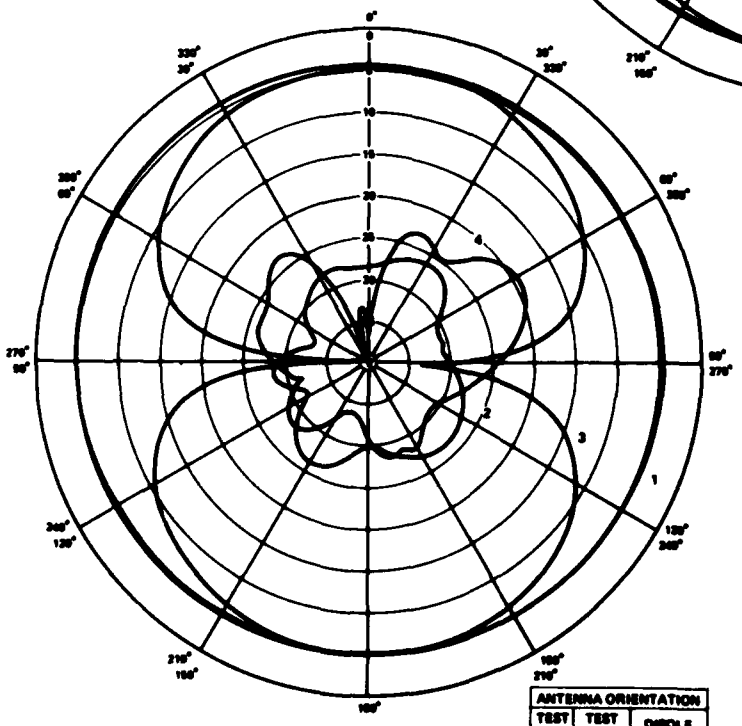

ANTENNA ORIENTATION		
TEST NO.	TEST LOOP	DIPOLE
1	HORIZ	HORIZ
2	HORIZ	VERT
3	VERT	VERT
4	VERT	HORIZ

Figure A-30. Loop antenna 670-2 radiation pattern measurements at 684 MHz.

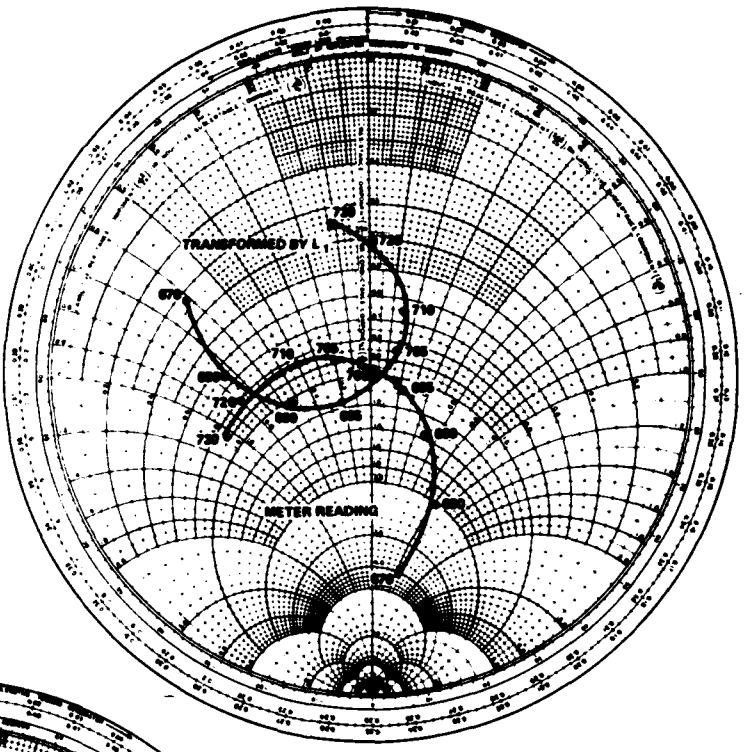

Figure A-31. Loop antenna 700-2 admittance measurements versus frequency in MHz.

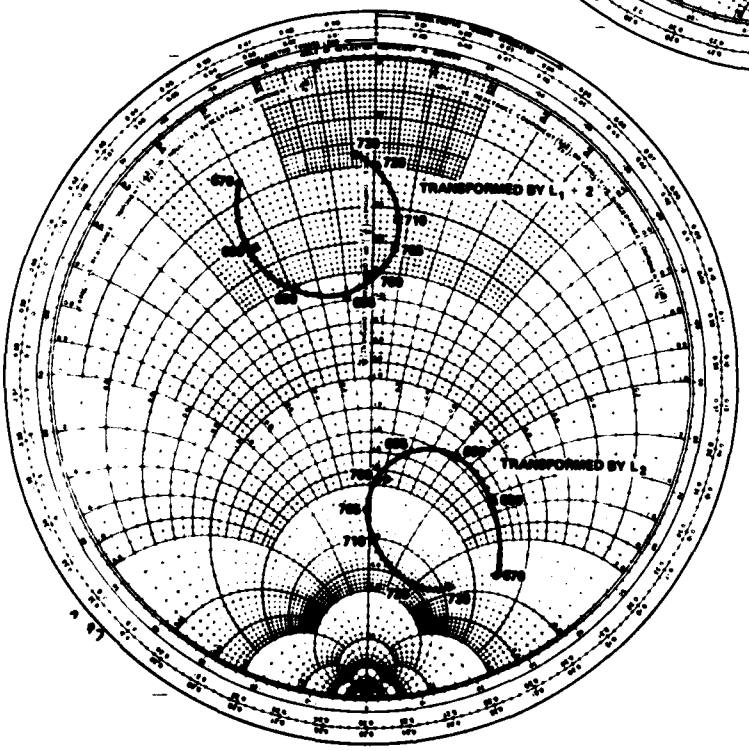

Figure A-32. Loop antenna 700-2 admittance measurements versus frequency in MHz.

APPENDIX A

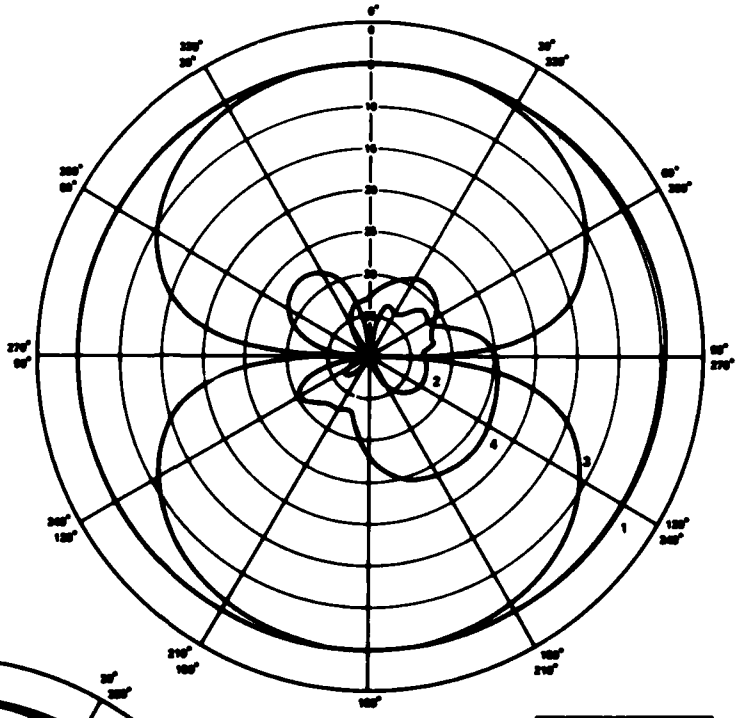

ANTENNA ORIENTATION		
TEST NO.	TEST LOOP	DIPOLE
1	HORIZ	HORIZ
2	HORIZ	VERT
3	VERT	VERT
4	VERT	HORIZ

Figure A-33. Loop antenna 700-2 radiation pattern measurements at 686 MHz.

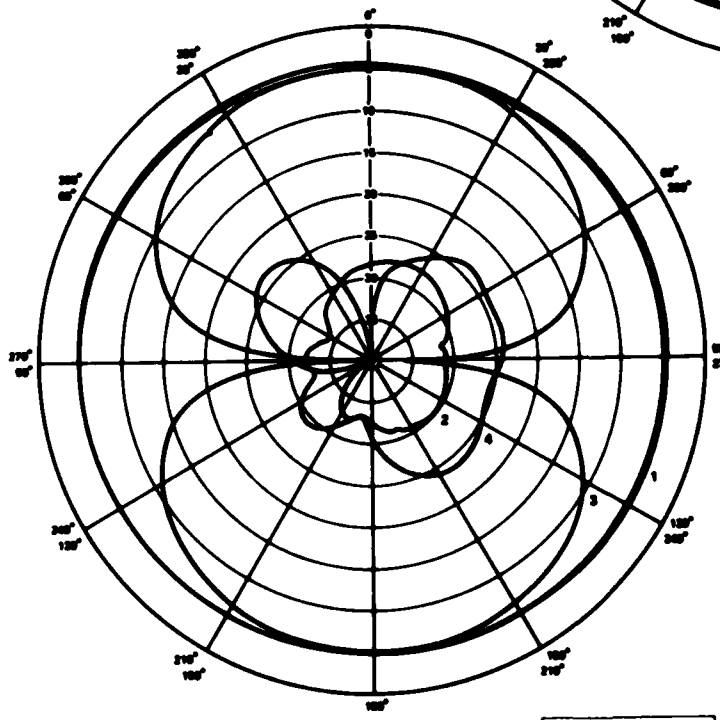

ANTENNA ORIENTATION		
TEST NO.	TEST LOOP	DIPOLE
1	HORIZ	HORIZ
2	HORIZ	VERT
3	VERT	VERT
4	VERT	HORIZ

Figure A-34. Loop antenna 700-2 radiation pattern measurements at 700 MHz.

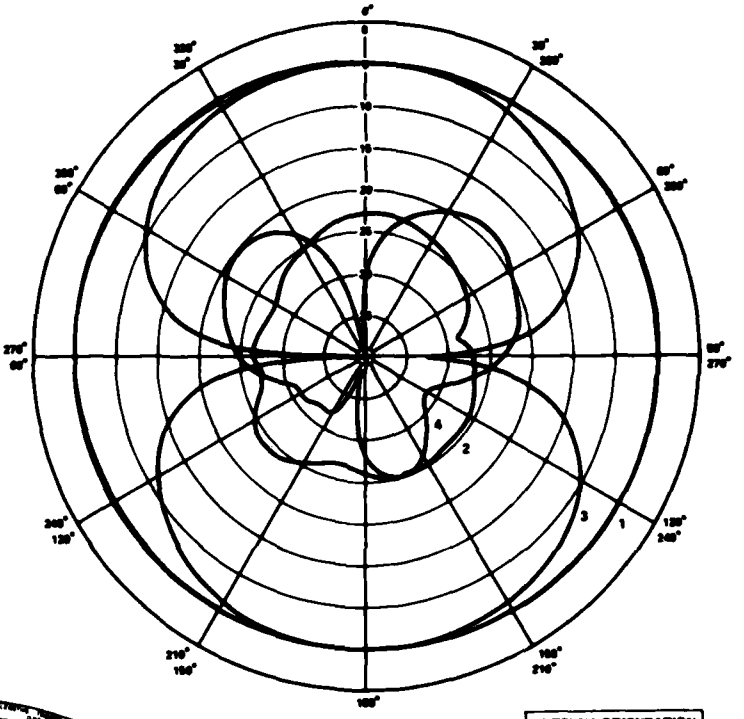

ANTENNA ORIENTATION		
TEST NO.	TEST LOOP	DIPOLE
1	HORIZ	HORIZ
2	HORIZ	VERT
3	VERT	VERT
4	VERT	HORIZ

Figure A-35. Loop antenna 700-2 radiation pattern measurements at 715 MHz.

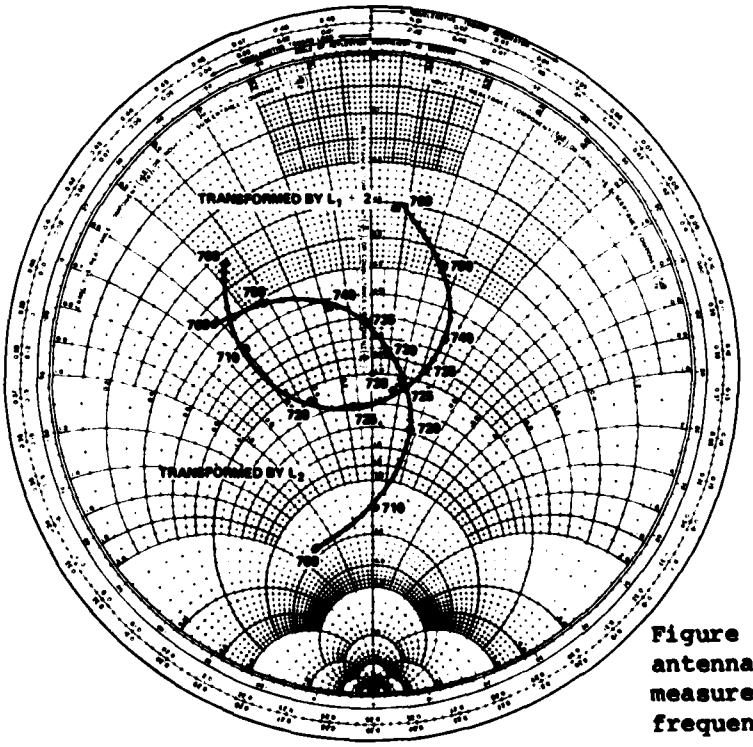

Figure A-36. Loop antenna 730-2 admittance measurements versus frequency in MHz.

APPENDIX A

Figure A-37. Loop antenna 730-2 admittance measurements versus frequency in MHz.

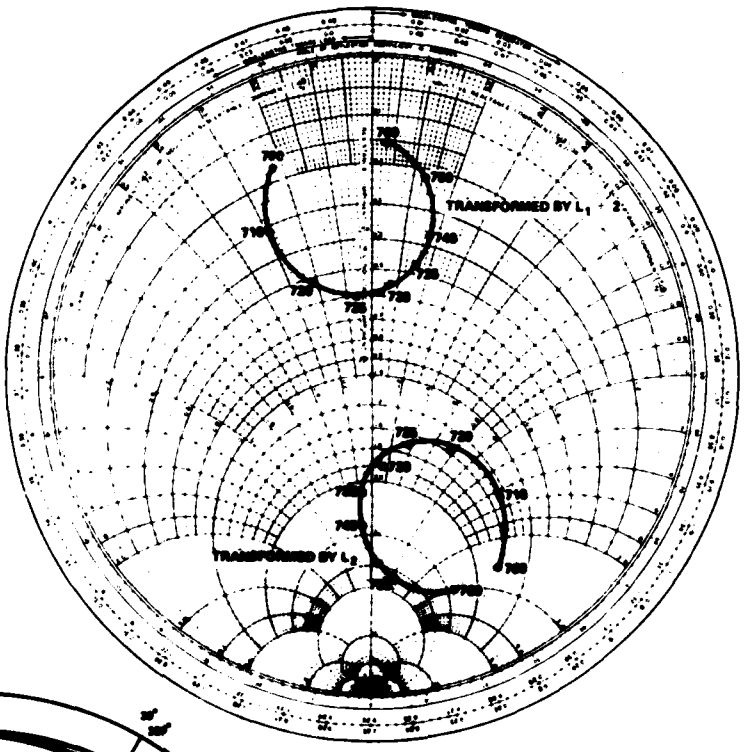

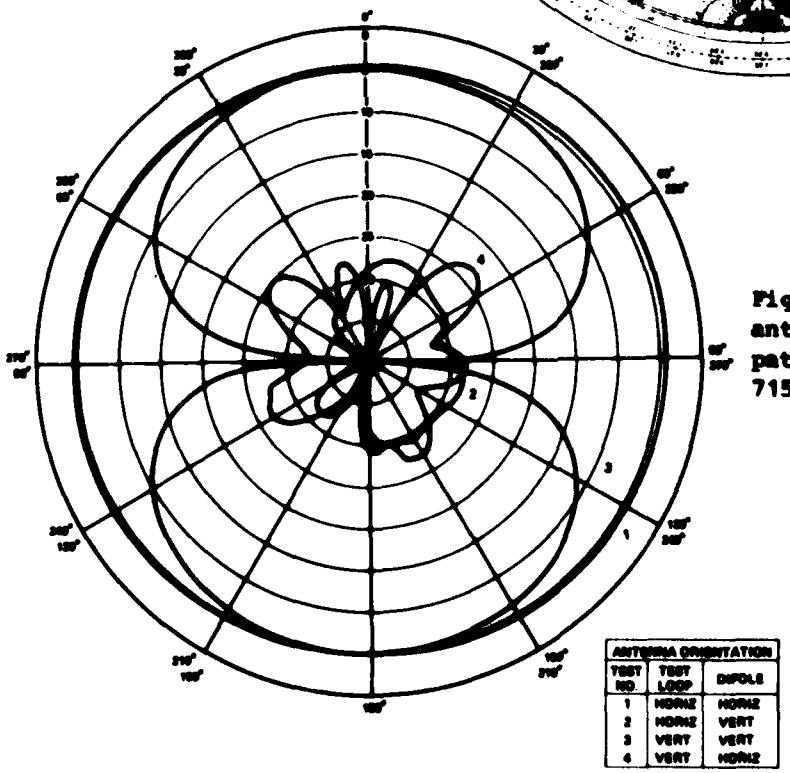

ANTENNA ORIENTATION		
TEST NO.	TEST LOOP	DIPOLE
1	HORIZ	HORIZ
2	HORIZ	VERT
3	VERT	VERT
4	VERT	HORIZ

Figure A-38. Loop antenna 730-2 radiation pattern measurements at 715 MHz.

Figure A-39. Loop antenna 730-2 radiation pattern measurements at 730 MHz.

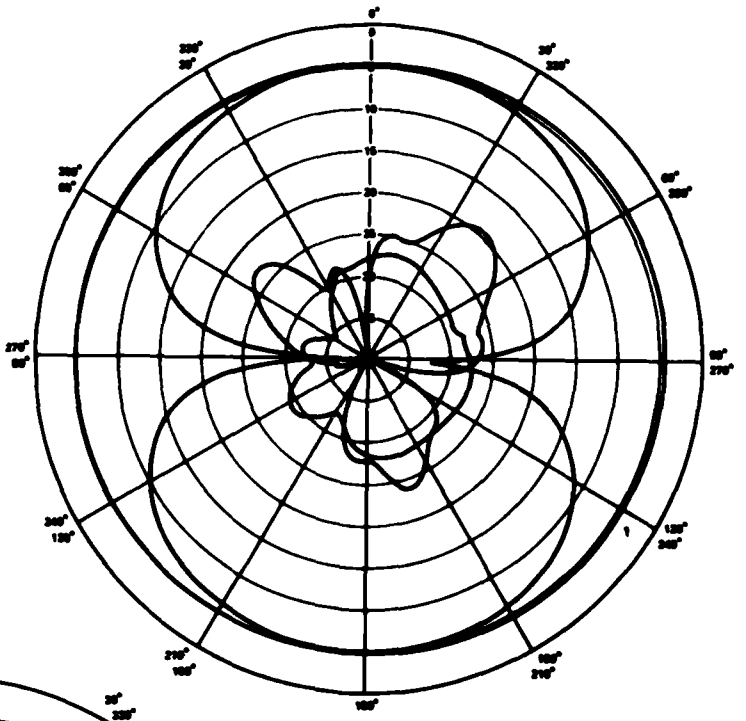

ANTENNA ORIENTATION		
TEST NO.	TEST LOOP	DIPOLE
1	HORIZ	HORIZ
2	HORIZ	VERT
3	VERT	VERT
4	VERT	HORIZ

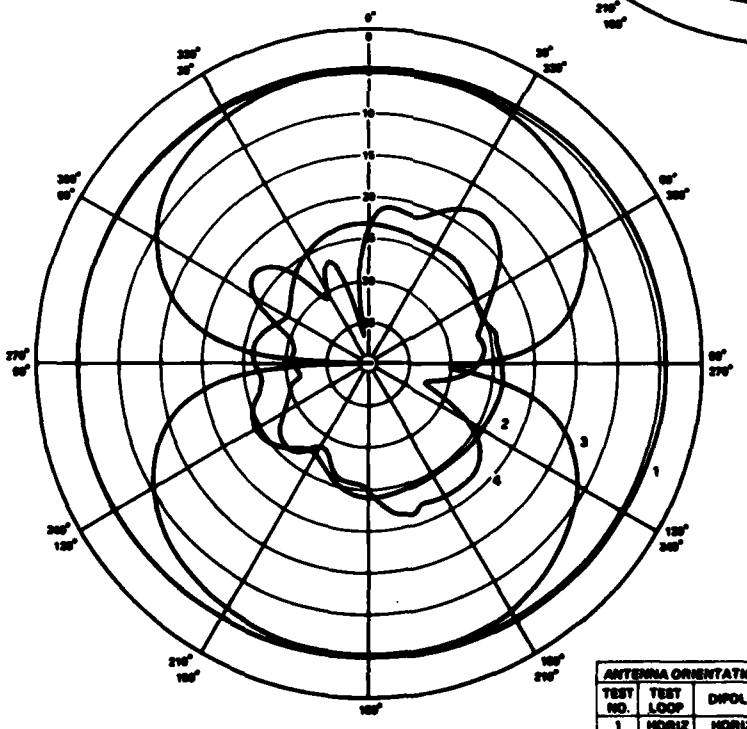

ANTENNA ORIENTATION		
TEST NO.	TEST LOOP	DIPOLE
1	HORIZ	HORIZ
2	HORIZ	VERT
3	VERT	VERT
4	VERT	HORIZ

Figure A-40. Loop antenna 730-2 radiation pattern measurements at 745 MHz.

APPENDIX B.--LOOP ANTENNA GAIN MEASUREMENTS PERFORMED AT THE NATIONAL BUREAU OF STANDARDS, BOULDER, CO

B-1. INTRODUCTION

All eight loop antennas were calibrated at the National Bureau of Standards (NBS) to determine the antenna gain at each specified frequency, and an estimate was made of the accuracy of the gain measurement.

B-2. NBS REPORT

The following is an excerpt from the letter report submitted by NBS dated 25 November 1975 on these gain measurements.

APPENDIX B COPY

The power gains of the antennas were determined to be:

Frequency (MHz)	Antenna No.	Gain (dB)	Antenna No.	Gain (dB)
617		.67 ± .4		.81 ± .5
630	630-1	.94 ± .4	630-2	1.14 ± .5
641		.98 ± .4		1.14 ± .5
657		.99 ± .4		.23 ± .5
670	670-1	.83 ± .4	670-2	1.19 ± .5
684		1.00 ± .4		.74 ± .5
683		1.28 ± .4		.54 ± .5
700	700-1	1.70 ± .4	700-2	.81 ± .5
713.5		1.56 ± .4		1.04 ± .5
718.5		.94 ± .4		1.10 ± .5
732.5	735-1	.40 ± .4	730-2	.75 ± .5
748		.31 ± .4		.99 ± .5

The error estimates are the result of a quadrature sum of the individual error components listed in the following tables. Each error component is a worst case or 3σ value and the errors are independent and uncorrelated.

Errors in Gain Measurement (Series XXX-1)

Source of Error	Resultant Error in Gain (dB)
Impedance Mismatch	.25
Aiming Errors	.05
Polarization Mismatch	.04
Proximity Error for Corner Reflector	.1
Error in Averaging Multipath	.1
Attenuator Calibration	.15
Distance Measurement and Choice of "phase center" For Corner Reflector	.1
Random Errors	.1
Quadrature Sum:	± .4

Errors in Gain Measurement (Series XXX-2)

Source of Error	Resultant Error in Gain (dB)
Uncertainty in Gain of "Standard"	.4
Impedance Mismatch	.25
Aiming Errors	.05
Polarization Mismatch	.04
Random Errors	.1
Quadrature Sum:	± .5

COPY

APPENDIX B

The power gain of the antennas was determined to be:

Antenna No.	Frequency (MHz)	Gain (dB)
630-2	617	.813 ± .6
	630	1.14 ± .6
	641	1.14 ± .6
670-2	657	.23 ± .6
	670	1.19 ± .6
	684	.74 ± .6
700-2	683	.54 ± .6
	700	.81 ± .6
	713	1.04 ± .6
730-2	718.5	1.10 ± .6
	732.5	.75 ± .6
	748	.99 ± .6

DISTRIBUTION

ADMINISTRATOR
DEFENSE TECHNICAL INFORMATION CENTER
ATTN DTIC-DDA (12 COPIES)
CAMERON STATION, BUILDING 5
ALEXANDRIA, VA 22314

COMMANDER
US ARMY RSCH & STD GP (EUR)
ATTN CHIEF, PHYSICS & MATH BRANCH
FPO NEW YORK 09510

COMMANDER
US ARMY ARMAMENT MATERIEL
READINESS COMMAND
ATTN DRSAR-LEP-L, TECHNICAL LIBRARY
ATTN DRSAR-ASF, FUZE &
MUNITIONS SPT DIV
ROCK ISLAND, IL 61299

COMMANDER
US ARMY MISSILE & MUNITIONS
CENTER & SCHOOL
ATTN ATSK-CTD-F
REDSTONE ARSENAL, AL 35809

DIRECTOR
US ARMY MATERIEL SYSTEMS ANALYSIS
ACTIVITY
ATTN DRXSY-MP
ATTN DRXSY-CC, COMM & ELECTRONICS
ABERDEEN PROVING GROUND, MD 21005

DIRECTOR
US ARMY BALLISTIC RESEARCH LABORATORY
ATTN DRDAR-TSB-S (STINFO)
ABERDEEN PROVING GROUND, MD 21005

US ARMY ELECTRONICS TECHNOLOGY
AND DEVICES LABORATORY
ATTN DELET-DD
FORT MONMOUTH, NJ 07703

HQ, USAF/SAMI
WASHINGTON, DC 20330

TELEDYNE BROWN ENGINEERING
CUMMINGS RESEARCH PARK
ATTN DR. MELVIN L. PRICE, MS-44
HUNTSVILLE, AL 35807

DIRECTOR
DEFENSE INTELLIGENCE AGENCY
ATTN DT-2, WEAPONS & SYSTEMS DIV
WASHINGTON, DC 20301

ASSISTANT SECRETARY OF THE ARMY
(RES, DEV, & ACQ)
ATTN DEP FOR SCI & TECH
WASHINGTON, DC 20310

OFFICE OF THE DEPUTY CHIEF OF STAFF
FOR RESEARCH, DEVELOPMENT & ACQ
DEPARTMENT OF THE ARMY
ATTN DAMA-CSC, ELECTRONIC WARFARE TM
WASHINGTON, DC 20310

COMMANDER
US ARMY ARMAMENT RESEARCH
& DEVELOPMENT COMMAND
ATTN DRDAR-LCF, FUZE DIV
DOVER, NJ 07801

DIRECTOR
ELECTRONIC WARFARE LABORATORY
FT MONMOUTH, NJ 07703

COMMANDER
OFC OF MSL ELECTRONIC WARFARE
WHITE SANDS MISSILE RANGE, NM 88002

COMMANDER
US ARMY MISSILE COMMAND
ATTM DRSMI-U, WEAPONS SYS MGT DIR
REDSTONE ARSENAL, AL 35809

DIRECTOR
NAVAL RESEARCH LABORATORY
ATTN CODE 5700, TACTICAL ELECTRONIC
WARFARE DIV
WASHINGTON, DC 20375

COMMANDER
NAVAL SURFACE WEAPONS CENTER
ATTN G40, GUZES & GUIDANCE SYS DIV
ATTN F42, RADAR SYS BR
ATTN F20, ELECTRONICS WARFARE DIV
WHITE OAK, MD 20910

COMMANDER
NAVAL WEAPONS CENTER
ATTN 33, FUZE DEPARTMENT
CHINA LAKE, CA 93555

DIRECTOR
AF AVIONICS LABORATORY
ATTN KL (WR), ELECTRONIC WARFARE DIV
WRIGHT-PATTERSON AFB, OH 45433

US ARMY ELECTRONICS RESEARCH
& DEVELOPMENT COMMAND
ATTN TECHNICAL DIRECTOR, DRDEL-CT

HARRY DIAMOND LABORATORIES
ATTN CO/TD/TSO/DIVISION DIRECTORS
ATTN RECORD COPY 81200
ATTN HDL LIBRARY (3 COPIES), 81100
ATTN HDL LIBRARY, (WOODBRIDGE), 81100
ATTN TECHNICAL REPORTS BRANCH, 81300
ATTN CHAIRMAN, EDITORIAL COMMITTEE

HARRY DIAMOND LABORATORIES (Cont'd)
ATTN LEGAL OFFICE, 97000
ATTN CHIEF, 21000
ATTN CHIEF, 21100
ATTN CHIEF, 21200
ATTN CHIEF, 21300
ATTN CHIEF, 21400
ATTN CHIEF, 21500
ATTN CHIEF, 20000
ATTN CHIEF, 22100
ATTN CHIEF, 22300
ATTN CHIEF, 22800
ATTN CHIEF, 22900
ATTN CHIEF, 20240
ATTN ARSEM, C., 11100
ATTN TOZZI, L., 11400
ATTN DAVID, J., 11400
ATTN STANN, B., 11100
ATTN CLASEN, S., 11200
ATTN INGERSOLL, P. 34300
ATTN BRANN, H., 47400
ATTN ISLER, W. E., 13500
ATTN GOODMAN, R., 34400
ATTN WILKIN, N., 22800 (10 COPIES)

END

DATE
FILMED

5-8

DTIC